UCRL-19129

c.2

JOINING TRIP STEELS

Sudhir Madhusudan Ambekar
(D. Eng.)

February 6, 1970

RECEIVED
LAWRENCE
RADIATION LABORATORY
MAR 23 1970
LIBRARY AND
DOCUMENTS SECTION

AEC Contract No. W-7405-eng-48

TWO-WEEK LOAN COPY

This is a Library Circulating Copy which may be borrowed for two weeks. For a personal retention copy, call Tech. Info. Division, Ext. 5545

LAWRENCE RADIATION LABORATORY
UNIVERSITY of CALIFORNIA BERKELEY

UCRL-19129

25

DISCLAIMER

This document was prepared as an account of work sponsored by the United States Government. While this document is believed to contain correct information, neither the United States Government nor any agency thereof, nor the Regents of the University of California, nor any of their employees, makes any warranty, express or implied, or assumes any legal responsibility for the accuracy, completeness, or usefulness of any information, apparatus, product, or process disclosed, or represents that its use would not infringe privately owned rights. Reference herein to any specific commercial product, process, or service by its trade name, trademark, manufacturer, or otherwise, does not necessarily constitute or imply its endorsement, recommendation, or favoring by the United States Government or any agency thereof, or the Regents of the University of California. The views and opinions of authors expressed herein do not necessarily state or reflect those of the United States Government or any agency thereof or the Regents of the University of California.

Contents

Abstract

I. INTRODUCTION ---------- 1

II. EXPERIMENTAL PROCEDURE: RESULTS ---------- 9

TIG Welding ---------- 10

Electron Beam Welding ---------- 11

Friction Welding ---------- 12

Metallography ---------- 13

III. DISCUSSION

Weld Strength ---------- 14

Weld Metallurgy ---------- 18

Subzero Treatment of Welds ---------- 20

IV. THEORETICAL ANALYSIS ---------- 23

Correlation of Results and Theoretical Model ---------- 28

V. SUMMARY AND CONCLUSIONS ---------- 30

APPENDIX

Welds in Bars of Circular Cross-Section ---------- 32

Joints Made in Plates ---------- 35

REFERENCES ---------- 38

ACKNOWLEDGEMENTS ---------- 39

TABLES ---------- 40

FIGURE CAPTIONS ---------- 42

JOINING TRIP STEELS

Sudhir Madhusudan Ambekar

Inorganic Materials Research Division, Lawrence Radiation Laboratory,
Department of Mechanical Engineering, College of Engineering,
University of California, Berkeley, California

ABSTRACT

A brief description of the properties and metallurgy of a TRIP steel (composition: 9 Cr - 8 Ni - 4 Mo - 2 Si - 2 Mn - 0.25 C) is given in order to gain an insight into the factors affecting weld strength and weld metallurgy.

The TRIP steel was welded by three processes (1) TIG, (2) electron beam, and (3) friction welding. The highest strength of 198 ksi was obtained by friction welding in a base metal having a yield strength of 207 ksi. Suggestions are made to further improve weld properties.

An approximate analytical model is presented to calculate the strength of butt welds in metals having a weld zone weaker than the base material. The model takes into account the strength gradient in the weld zone and computes the strength based on the dimensions of the joint, the width of the weld zone and the strengths of the base metal and the weld zone. Experimental results substantiate the theoretical model.

I. INTRODUCTION

Two of the most common ways of increasing the yield and tensile strength of steels are heat treatment and mechanical processing. However with such treatments an increase in the yield and tensile strengths causes a decrease in the uniform elongation to fracture. The stress strain curves of such alloys are "flatter" at higher plastic strains. Further, they lack the ability to yield locally and redistribute stresses at notches and other unavoiable stress raisers in structural applications.

In studying the mechanical properties of a metal, reduction in area is a more meaningful measurement of ductility than elongation. A literature survey in this field shows that the elongation drops more rapidly than the reduction in area as the yield strength of an alloy is increased by heat treatment or mechanical processing.

Many steels having yield strengths well over 200,000 psi have reductions in areas of 50% or more. It is thus evident that local necking is responsible for the low values of elongation exhibited by many high strength alloy steels and that if necking could be suppressed then the total elongation would be enhanced. It is also observed that in quenched and tempered low alloy steels that the higher the tensile (and yield) strengths, the lower is the tensile strain at which necking begins but the true-strain-true-stress curves are essentially parallel. This means that the strain hardening by dislocation interactions is substantially independent of the yield strength, but is inadequate to compensate for the increase in stress in the region of the neck. Therefore, if the inherent ductility (as indicated by the reduction of area) is to be utilized in the form of uniform plastic strain, barriers stronger

than dislocation tangles must be formed during plastic straining (as opposed to before plastic straining which would increase the yield strength but not necessarily the strain hardening rate). Martensite plates can act as strong barriers to dislocation motion, particularly when the carbon content exceeds about 0.2% (1). This together with the knowledge of strain induced martensite transformation led to the development of TRIP steels. (TRIP is an acronym for TRansformation Induced Plasticity).

McEvily and Busch (2), Gerberich, Martin and Zackay (3), and Thomas, Schmatz and Gerberich (4) have concluded that some austenites containing carbon and a carbide-forming alloying element can undergo austenite decomposition when deformed above room temperature but below the recrystallization temperature. In steels containing strong carbide formers, alloy carbides can precipitate on an extremely fine scale during deformation above the M_D temperature. This fine dispersion of carbides, and subsequent deformation and transformation to martensite below the M_D temperature are responsible for the high yield strengths of ausformed steels. The precipitation of carbides causes a depletion of carbon in the surrounding austenite thereby raising the M_s and M_D temperatures. (M_s is the temperature below which austenite transforms to martensite by cooling alone. M_D is the temperature below which austenite transforms to martensite by plastic deformation alone). For steels the M_D temperature is approximately 50-100°F above the M_s temperature.

The high yield strength of TRIP steels comes from the high dislocation density introduced by prior working. However, the precipitates formed during deformation also govern the strength and other mechanical

properties to a considerable extent.

As austenite is cooled, its stability, relative to martensite of the same composition, decreases. Below the M_s temperature, the austenite is sufficiently less stable so that martensite is formed. Most alloying elements in steels lower the M_s temperature. Precipitation of carbides, identified as MoC and Cr_2C_3 by Fahr (5), causes a depletion of alloying elements in the matrix and consequently reduces the stability of the austenite.

Mechanical deformation on the other hand stabilizes the austenite. The M_s temperature is decreased with increased amounts of deformation making the austenite more stable. This is attributed by Fahr (6) to the subdivision of the austenite grains into small cells bounded by carbide plates which limit the size and the amount of martensite plates formed. It is found that the stabilizing effect of prior deformation on austenite is more predominant than the opposing effect of precipitation.

In a tension test of TRIP steel, shortly after the elastic limit is reached there is a yield point phenomenon coincident with Luder's band formation in the gage section. The austenite at least partially transforms into martensite. Strain hardening occurs in the yielded band only and not outside it. As a result flow takes place in the adjacent layers and in this the Luder's band traverses the gage section. The yield front now traverses back along the gage section and the strain hardening rate increases rapidly as it encounters the hard martensitic phase. This process continues until the gage section is almost all martensitic at which time maximum load is reached and failure

ensues. In this case the strain-induced martensite enhances the local work hardening rate and prevents premature necking. For high strength materials the local work hardening rate must be quite high to suppress necking. It is for this reason that most high strength steels, e.g., SAE4340 and 18 Ni maraging steels with low work hardening rates neck shortly after yielding.

The TRIP phenomenon also improves the resistance of TRIP steels to crack propagation and thus improves fracture toughness. Austenite-martensite transformation occurs ahead of the crack tip in the plastic zone, and this is an energy dissipation mechanism. It has been shown (7) that the degree of energy dissipation from this mechanism may be greater than other plastic deformation processes. The same general explanation is given for their high resistance to crack propagation under fatigue conditions.

Although the TRIP phenomenon can be observed in large numbers of alloy combinations, investigations at the Inorganic Materials Research Division of the Lawrence Radiation Laboratory show that the best mechanical properties are observed in the following compositions (8).

(A) 9 Cr - 8 Ni - 4 Mo - 2 Si - 2 Mn - 0.25 C

(Good room temperature properties)

(B) 13 Cr - 9 Ni - 3 Mo - 2 Mn - 0.20 C

(Good low temperature properties)

The thermomechanical treatment consists of homogenizing, forging, and annealing the ingots to destroy the original cast structure and then warm rolling above the M_D temperature to produce an austenite having yield strengths of more than 200,000 psi.

The mechanical properties of TRIP steels can be made to suite specific applications by appropriate changes in the chemical composition, amount of prior deformation and processing temperatures.

From the foregoing discussion it may be inferred that the thermo-mechanical treatment has a twofold purpose in the preparation of TRIP steel. It increases the yield strength by introducing warm work and it also stabilizes the austenite. When such a steel is heated to a temperature above its recrystallization temperature and cooled to room temperature, the opposite effect takes place. It loses its high yield strength and the austenite becomes less stable. Thus it is clear that a fusion weld in TRIP steel would have poor joint efficiency. (Joint efficiency is defined as the ratio of the ultimate strength of the welded joint to the ultimate strength of the base metal. If the joint fails in the base metal the joint efficiency is assumed to be 100%.)

When the metals being joined are not critically heat sensitive, proper shielding, alloying of the fusion zone and careful control of the welding process usually result in relatively high joint efficiencies. But when a heat-sensitive metal, like TRIP steel, is welded and tested in tension the plastic deformation is limited to the weld zone (the fusion and the heat affected zone) only and the failure would be expected to occur in this region. Hence although locally the strain in the weld zone may be quite high, the overall elongation of the joint is very low. If it were possible to achieve a joint strength equal to or greater than the ultimate strength of the base metal, the base metal would yield and for most practical purposes the mechanical properties of the joint would be the same as those of the base metal. Hence ideally,

the weld zone should have a very high strain-hardening rate so as to produce base metal yielding, thereby resulting in larger uniform elongations before fracture. This is essential to realize the full practical potential of the TRIP steels.

The most obvious approach is to add alloying elements to the fusion zone, by means of a filler metal, to produce the required mechanical properties. However, there is always a heat-affected zone (HAZ), adjacent to the fusion zone. This zone does not melt at any time but merely undergoes a metallurgical transformation as a result of the heating and cooling during the welding process. Consequently, in heat sensitive metals the mechanical properties of the heat affected zone are far inferior to the base metal properties. In some alloy steels the properties can be restored by post-weld-heat treatment. However, when the properties of the base metal are derived from prior deformation it is difficult if not impossible, to restore these properties by heat treatment. The heat affected zone in such cases consists of austenite that is recrystallized and the beneficial effects of the cold work have consequently been destroyed. If the TRIP steel has a high carbon content it may be possible to quench the weld to below the M_s temperature of the recrystallized austenite to produce martensite. This high carbon martensite has a high yield strength and strain hardening rate. However, since post-welding thermomechanical treatment is usually not feasible, there is no simple way of improving the strength of such joints. The most obvious alternative process would be a diffusion or a solid state bonding process where the temperatures involved will not cause any phase change or recrystallization with consequent deterioration of

properties. However, the applicability of such a process is very restricted especially if vacuum conditions and/or special surface preparations are required.

One means of increasing the strength of such butt-welded joints is to limit the width of the weld zone, thereby developing hydrostatic tension in the narrow softened zone due to the constraint imposed by high strength base metal. This mechanism is similar to that in a brazed joint; the narrower the weld zone, the higher the yield strength. In brazed joints however, the thickness of the brazing alloy is usually much smaller compared to the physical dimensions of the parts being joined than is possible by any current fusion welding process.

Nikolajs Bredzs (9) who studied the variation of tensile strength of brazed joints with joint thickness, concluded that the increase in the tensile strength with decrease in joint thickness is due almost exclusively to the increase of the biaxial constraint and the suppression of the neckdown effect of the filler metal. It has long been recognized that the tensile strength of a metal may be increased by increasing the biaxial constraint in tension tests of notched bars. In brazed joints, since the strength of the brazing alloy is far less than the strength of the base metal, the effective strength of the constrained brazing alloy may thus be raised many times its strength in uniaxial tension, and this is dependent upon the geometry of the joint.

These investigations of brazed joints may be applied to welded joints when the fusion zone and the heat affected zone are weaker than the base metal. However since the width of even the most narrow weld zone is much greater than a brazed joint, the constrained weld zone

strength cannot be increased to the same extent. However, the strength of the weld zone is relatively high compared to a brazing alloy and a small decrease in the width of the weld zone increases the weld strength considerably. In most cases it may be only necessary to increase the strength of the constrained weld zone by a factor of 2 to 2.5 times to reach the yield strength of the base metal.

Once the base metal has yielded, the strength of the joint is the same as that of the base metal (assuming no strain hardening in the base metal).

The experiments described herein were performed with this as the goal. Later in the discussion an approximate analytical model is presented to calculate the strength of the joint. Although the experiments were not performed with the objective of proving the validity of the theoretical model, results obtained do substantiate the proposed model and analysis.

II. EXPERIMENTAL PROCEDURE: RESULTS

As stated earlier, there is no one single typical TRIP steel composition. The occurrence of the TRIP phenomenon depends upon the proper balance of the alloying elements and the thermomechanical treatment. The composition and treatment chosen for this study was the one that has good room temperature properties. Several heats of the same nominal composition

9 Cr - 8 Ni - 4 Mo - 2 Si - 2 Mn - 0.25 C

were melted in either vacuum or inert atmosphere and poured into heavy copper molds. The subsequent treatment consisted of homogenization for three days at 2000°F and forging at 2000°F to the required size before final warm deformation. (Care was taken to eliminate the original cast grain structure by upsetting and cross forging, thereby preventing cracking in the subsequent warm rolling operation.) Forging was followed by austenitization at 2200°F for 3 hours and quenching in an ice-brine solution. This annealed material was then warm rolled 75-80% at 840°F. For sheet stock, the ingots were forged to a rectangular slab and then rolled, while for round bars the ingots were forged round and rolled between form-rolls.

The tension specimens used are shown in Figs. 1 and 2. These were tested in an Instron machine with a cross-head speed of 0.04 in./min. The room temperature stress-strain curves of the base material are shown in Fig. 3 and Fig. 4.

The first experiments were made to determine the effects of various heating cycles on the properties of the material. A fast temperature rise for sheet specimens was achieved by resistive heating. The

temperature cycle was recorded by small diameter (0.003 in. diameter) chromel-alumel thermocouples attached to the maximum temperature zone. The specimens were air-cooled. These heated specimens were then tension tested at room termperature. The variation of yield stress and ultimate tensile stress with maximum temperature of heating is shown in Fig. 5.

The graph shows a sharp drop in the yield strength beyond 1300°F which corresponds to the recrystallization temperature of the deformed austenite. Microhardness measurements were made on these specimens and a graph of microhardness vs yield strength is shown in Fig. 6. Tensile strengths may also be correlated with hardness measurements. However, it was necessary to relate microhardness to the yield strength so that the data could be used to check the validity of the theoretical analysis later.

TIG Welding

Fusion welding of TRIP steel without the addition of filler metal was then undertaken using the Tungsten Inert Gas (TIG) welding process on 1/16 in. thick sheet stock. In all sheet metal welds any "build-up" was ground off before tension testing. Tension test specimens were machined with the weld in the middle of the gage section and the resulting stress-strain curve is shown in Fig. 7. A microhardness traverse across the weld zone before tension testing is shown in Fig. 8 which gives an indication of the weld zone width and strength of both the fusion zone and the HAZ.

A similar weld was then made using a maraging steel filler metal, having a nominal composition of 18 Ni, 8 Co, 5 Mo, 1 Ti, and was introduced in the weld in the form of 1/8 in. rod. The weld was then aged

at 930°F for 6 hours. The tensile stress-strain curve for such a weld is shown in Fig. 9 and the microhardness traverse across the weld zone is given in Fig. 10. The specimen necked on both sides of the fusion zone and failed in one of the necks. The fracture stress in this case is somewhat greater than that in a simple TIG weld.

Electron Beam Welding

Production of a narrow weld zone requires a highly concentrated heat source. Other conventional processes using an arc as the heat source are comparable to or worse than the TIG process in this respect. However the electron beam does offer such a concentrated heat source. Therefore, in an attempt to further reduce the width of the soft zone, an electron beam weld was made without filler metal. Welding was done under vacuum conditions at 1×10^{-4} Torr and a travel speed of 30 in./min. The stress-strain curve of this weld is shown in Fig. 11 and the microhardness traverse across the weld is given in Fig. 12.

Finally, an attempt was made to introduce filler metal into the electron beam butt weld. The filler metal was introduced in the form of strips of maraging type steel sandwiched between two ends of the TRIP steel members being joined. The electron beam was defocussed to fuse the strip and the base metal together. This weld was also tested in tension and the resulting stress-strain curve is shown in Fig. 13 while the microhardness traverses is shown in Fig. 14.

In order to determine the strength of a weld at a temperature far below the M_D temperature of the annealed austenite, an electron beam weld (without filler) was tested at liquid nitrogen temperature. The stress-strain curve of such a specimen is shown in Fig. 15.

Friction Welding

Friction welding was tried on round bars in an effort to minimize the heat affected zone and induce warm working during the welding cycle. Specimens used for these experiments are shown in Fig. 16 and the process is described briefly below:

Friction welding is a welding process wherein coalescence is produced by frictional heat derived from sliding motion between two surfaces held together under pressure. Conventional friction welding rotates one part at relatively high controlled speeds against a stationary member to which it is to be joined. The weld is completed within seconds or less, after making contact. This results in a comparatively narrow heat affected zone. Filler metal, fluxes or shielding gases are not required in this process and welds can be made with a minimum of work piece preparation.

The variables to be controlled are

a) rotational speed

b) axial weld pressure

c) amount of upset or axial shortening of the assembly (the length of welding time or number of revolutions of the rotating member may be substituted for this)

d) forge pressure (pressure applied for a predetermined time after the weld cycle is completed).

Provisions were made on the machine used to record torque, axial pressure, and actual "upset".

The interface reaches a high temperature as a result of friction between the rotating and stationary members. As a consequence the

metal at and in the vicinity of the interface becomes soft and flows outward. Such action separates or removes surface impurities, thus bringing metallurgically clean surfaces into contact, thereby creating a sound metallurgical bond with a minimized width of the heat affected zone.

Properties of the welds produced are determined to a considerable extent by the various process parameters, and optimum process conditions require extensive experimentation. However, in the present study an effort was made to reduce the number of variables by utilizing information that previous experiments had shown to be an adequate amount of upset (0.030 in.) and forge time (4 sec).

Welds were made in 1/4 in. diameter specimens after which they were machined to eliminate any eccentricity. Tension test results of some of these welds are shown in Table I. The stress strain curve for a representative friction weld is shown in Fig. 17 and the microhardness traverse for a similar specimen is shown in Fig. 18. Figure 19 shows the stress strain curve of a friction weld where there is considerable yielding of the base metal and Fig. 20 shows the corresponding microhardness traverse on the weld.

Metallography

The welded specimens were mounted in bakelite, polished mechanically and etched by swabbing with Kalling's reagent (5 gm Cupric Chloride, 100 ml HCl, 100 ml alcohol and 100 ml water). A Carl Zeiss optical microscope was used for observation and photography of the welds. Most of the micrographs were taken at a magnification of 600×, so that a comparative study of the structure could be made.

III DISCUSSION

Weld Strength

It is evident from Fig. 5 that the room temperature yield strength of the material heated to different temperature remains essentially constant until about 1000°F. Between 1300°F and 1400°F the yield strength decreases very rapidly and the decrease becomes more gradual at higher temperatures. The relationship between microhardness and yield strength is shown in Fig. 6 and is approximately linear in the temperature range below the recrystallization temperature, but in the vicinity of the recrystallization temperature the yield strength drops rapidly whereas the hardness is essentially constant.

Microhardness traverse across the weld zones clearly demonstrates that the weld zone consists of a weak central region (fusion zone). On both sides of this zone there is a region (heat affected zone) in which there is a strength gradient. When such a weld is tested in tension it behaves like a composite material. Looking at the stress-strain diagram (Fig. 7) of the TIG weld it may be seen that there are two distinct stages of deformation. In the first stage, both the base metal and the weld zone are in the elastic stage. In the second stage the weld zone is in the plastic range while the base metal is still in the elastic range. The resulting curvature is a composite of the slopes of the elastic curve of the base metal and the plastic curve of the weld zone. Strain hardening in this second stage is determined almost entirely by the strain hardening characteristics of the weld zone since the slope of the elastic curve of the base metal is essentially constant. If the weld zone has a high rate of strain hardening it may be possible to

to cause the base metal to yield before fracture occurs in the weld zone. However in this case the weld zone is made up of annealed and cast TRIP steel and the properties of the weld zone are governed by the composition and metallurgical state of the TRIP steel. The width of the weld zone is approximately 0.45 in. (Fig. 8) in specimen 1/16 in. thick and 1/8 in. wide. Therefore the mechanical constraint exercised by the base metal is relatively small. The stress-strain curve deviates from linearity at approximately the yield stress (70,000 psi) of annealed TRIP steel but the fracture stress is 118,000 psi.

In the case of a similar weld made with the maraging type steel as filler metal the total width of the weld zone is approximately the same (0.40 in.) as shown in Fig. 10. However the fracture strength is 140,000 psi (Fig. 9 approximately 17% higher than the TIG weld without filler metal. From Fig. 10 it is clear that the maraging type steel fusion zone is much stronger than the heat affected zone in the base metal. Effectively then, the strong fusion zone divides the weld zone, thereby separating the two weak heat affected zones. The mean width of the two heat affected zones is approximately 0.125 in. The relatively strong maraging steel deposit and the base metal exercise mechanical constraint on the deformations of the heat affected zones resulting in higher strength. The weld deforms plastically on both sides of the fusion zone and fails in one of the two regions.

It should be mentioned at this stage that since the weld failed in the heat affected zone and not in the fusion zone, alloying would not increase the properties of the weld zone. The strength of such a weld is determined entirely by the width and the strength of the heat

affected zone, and there is no simple method of improving the properties of this region since the strength of TRIP steels is derived from warm work. The effect of subzero treatment of welds is discussed later.

An electron beam weld is similar to the TIG except the weld zone is much narrower. Both have a cast structure and heat affected zones. It is unquestionable that generally the electron beam weld cools faster but a comparative study of the microhardness traverses shows that the weakest section in both have approximately the same hardness. (See Figs. 8 and 12.) The weld fails in the fusion zone in a brittle manner. Fracture stresses are quite high, 146,000 psi (Fig. 11) in 1/16 in. thick by 1/8 in. wide specimens. The width of the weld zone is approximately 0.080 in. (Fig. 12). Although pure plane strain conditions are not obtained under these conditions, there is considerable increase in the yield stress of the weld zone. Electron beam welding under carefully controlled conditions probably produces the narrowest weld zone of any conventional welding process. The next obvious move is to split the weld zone as discussed earlier by adding filler metal. The effect of filler metal in the electron beam weld is similar to that in the TIG weld, but the increase in strength is a smaller fraction.

Friction welding with its inherent limitations as far as application is concerned, still offers a method of obtaining very high joint strength. It is one of the few processes that offers a controlled forge cycle. This may be utilized to induce cold work into the weld junction. The forge cycle also helps to refine the grain structure. In most conventional fusion welding processes the hottest (and consequently the weakest) metal is retained but in friction welding most of the high

temperature region is forced out in the form of flash, and subsurface layers are brought into contact. Although whether bulk fusion actually occurs in friction welding is still a subject of controversy, microhardness traverse shows that the weakest region in the weld is still much harder than the cast structure produced by conventional fusion processes (Fig. 18). It may be possible that the molten metal is thrown out in the form of flash and a bond is formed by intimate contact of nascent subsurface layers. It may be assumed that flash forms when the local flow stress of the metal at the interface falls just below the applied axial weld pressure and the yield strength of the region at the new interface is greater than or equal to the axial weld pressure. Consequently, higher weld pressures result in stronger and narrower weld zones giving rise to higher joint strengths. This is evident in Table I. Thus sufficient weld pressure is essential for a good bond. Insufficient weld pressure gives rise to voids in the welds resulting in premature failure.

In this experiment it was found that the forge pressure was not effective in increasing the strength of the weld zone. This may be because either the forge pressure "hot works" the weld zone or it is not sufficient to impart cold work. The axial pressures are limited by the capacity of the machine and the size of the members to be joined.

It is interesting to note that strength of the joint in Fig. 19 closely approaches the yield strength of the base metal and is therefore more ductile (8% uniform plastic elongation) than the joint in Fig. 17 which is less strong and shows practically no uniform plastic elongation to fracture.

Weld Metallurgy

The TIG welds and the electron beam welds are basically similar with the effects of intense heat more pronounced in the former. Figure 21 shows the microstructure of the base metal. It shows the carbides that are precipitated during rolling. Figure 22 shows the fusion zone in the TIG weld. It is basically a cast cored structure. Figure 23 shows the boundary between the fusion zone and the heat affected zone; when compared with Fig. 21, the tremendous grain growth in the heat affected zone can be appreciated. Since TRIP steel has a face centered cubic structure at room temperature, annealing twins may be expected in the heat affected zone. Evidence of such twins is found in Fig. 24 which also shows the heat affected zone close to the weld. The fusion zone and the heat affected zone close to it reaches temperatures sufficently high to dissolve carbides and there is no evidence in optical microscopy of any significant amount of precipitation during cooling.

However, further away from the fusion zone there is a region where the temperature reached during welding enhances precipitation and growth of the carbide particles. This region is shown in Fig. 25. It is analogous to the sensitized region in stainless steel welds. The carbides in TRIP steel have been identified by Fahr (5) to be those of chromium and molybdenum.

The structure of the heat affected zone and the fusion zone in TIG welds with a maraging steel filler is similar to that in a simple TIG weld with no filler. The fusion zone, however, consists of two parts. The central region where there is a large concentration of the filler and the region next to it where there is more mixing and consequently

a lower concentration of the filler metal. Figures 26 and 27 show these two regions respectively in the aged condition. The darker regions in the micrographs are the maraging steel filler regions. The central hard region helps to divide the weld zone into two parts as discussed earlier. The region where the concentration of the filler metal is less, behaves like a two-phase region; hard maraging steel regions dispersed in soft austenite. This region would be expected to have a higher strength and strain hardening rate like a composite material.

The fusion zone (Fig. 28) in the electron beam weld is a cast zone, with a dendritic cored structure that is much finer than in the TIG weld, (Fig. 26). The boundary of the fusion zone is clearly defined as seen in Fig. 29. The heat affected zone is limited in width when compared to the TIG weld as a consequence of the more concentrated heat input, faster cooling rate, and faster travel speed. Evidence of annealing twins in the heat affected zone are also evident in this case, (see Fig. 29). Further away from the fusion zone there is again a region of carbide precipitation and growth, (see Fig. 30). The fusion zone of the electron beam weld with filler is shown in Fig. 31.

The structure of the friction weld is complicated by the fact that mechanical deformation accompanies weld formation and that the temperature is not uniform across the weld interface. The periphery of the specimen has the highest surface speed and consequently is a high temperature region. The central region on the other hand has a low surface speed and hence is at a comparatively low temperature. The high temperature region has a low flow stress, therefore it undergoes intense deformation. The opposite is true for the central region. High temperature, together

with plastic deformation, enhances diffusion rate and precipitation. Figure 32 shows the interface and its vicinity of a friction weld at a magnification of 95X. The interface is wider near the outer periphery (top of the photograph). The dark bands may be caused by precipitates and/or deformation lines. In the central region, plastic deformation is very limited, however the microhardness traverse along the center line (Fig. 20) shows a slight increase in the hardness. Hence it may be inferred that carbide precipitation predominates in the central region, (Fig. 33). Since the region near the outer periphery is at a higher temperature, there is less concentration of carbide particles, (Fig. 34). Figure 35 shows grain flow in a region further away from the interface. The dark bands in this case are a result of both plastic deformation and precipitation. However, the deformation takes place above the recrystallization temperature; consequently, there is no strengthening effect.

Micrographs of the friction weld do not show any evidence of a "fusion zone". The grains in the heat affected zone are severely deformed as a result of the combined effects of high temperature, rotation, and axial pressure. These factors together with the fact that the weld is formed in a very short time (approximately 0.5 sec in this case), increase the strength and decrease the width of the softened zone.

Subzero Treatment of Welds

This particular TRIP steel, in the annealed state, has an M_s temperature slightly higher than the temperature of liquid nitrogen. It is, therefore, not possible to transform the recrystallized and cast austenite in the weld zone to martensite to any significant extent by

quenching in liquid nitrogen. However, if the alloy content (especially manganese) of the steel is reduced so that the M_s temperature of the warm-rolled TRIP steel is below the liquid nitrogen temperature and that of the annealed austenite is above it, the weld zone could be transformed to martensite by such quenching. The martensite thus produced will increase the weld zone strength. Thus it may be concluded that in principle, at least,it is possible to strengthen the weld zone by quenching it to a temperature intermediate between the M_s temperatures of the warm worked austenite and annealed austenite. It is usually desirable to have a large difference between the M_s and M_D temperatures of TRIP steel so that strain induced transformation can be obtained over a wide range of temperatures. Large amounts of warm work increase the yield strength of the TRIP steel and also increase the difference between the M_s and the M_D temperatures by decreasing the M_s temperature of the austenite. A smaller alloy content on the other hand will tend to increase the M_s temperature of the annealed austenite. Thus, large amounts of warm work and a smaller alloy content will increase the difference between the M_s temperatures of the warm worked and annealed austenites making the sub-zero treatment of welds more practical.

Testing of the electron beam weld at liquid nitrogen temperature (Fig. 15) suggests another approach for obtaining high strength welds. If the service temperature of the weld is well below the M_D temperature of the annealed austenite, the amount of martensite formed per unit strain is much higher thus increasing the strain-hardening rate and the strength of the joint. In Fig. 15 however, the effect of the cryogenic temperature makes the weld brittle. Thus it may be concluded that

proper alloying of the TRIP steel itself will help toward obtaining a stronger weld.

IV. THEORETICAL ANALYSIS

A theoretical analysis will be made first for the case where the properties are uniform across the weld zone and then later modified to account for gradual change in properties across it. The following assumptions have been made.

1. The weld is considered as a layer of soft metal sandwiched between the ends of two pieces of higher strength metal; (see Fig. 36).

2. The elastic moduli are equal for both metals.

3. Poisson's ratios are equal for both metals.

4. Plastic deformation is limited to the weld zone and there is no strain hardening of the weld zone.

5. No residual stresses are present.

6. The weld has no defects and the bond between the hard and the soft metal is metallurgically sound.

7. Initial failure of the weld zone starts when the shear stress at the interface (between the hard and the soft metal) reaches the shear yield point of the weld zone.

The first assumption simulates the weld and is a valid approximation when the strength of the fusion and heat affected zones are lower than the strength of base metal.

The second and third assumptions will generally be valid for welds between similar metals. Although the yield strength of the base metal and weld zone, may be quite different, their elastic moduli and the Poisson's ratio will be quite similar. This assumption simplifies the analysis as the radial stresses arising from differences in mechanical properties do not have to be considered.

The fourth, fifth, and the sixth assumpions are for mathematical simplicity.

The failure criterion is reasonable since the interface experiences maximum shear. It is consistent with the assumption that there is no strain hardening in the weld zone.

Under these assumptions, the breaking strength σ_b, of the welds in round members is given by

$$\sigma_b = \sigma_w \left[1 + \frac{1}{3\sqrt{3}} \cdot \frac{D}{h} \right] \qquad \text{(I)}$$

where σ_w is the yield strength, D the diameter and h the width of the weld zone. For details of this derivation the reader is referred to the appendix. It should be noted that this expression does not involve the yield strength of the base metal in a welded joint. It only assumes that the base metal is stronger than the weld zone, and that it does not yield. If the ratio, D/h is so high that the calculated strength of the joint exceeds the yield strength of the base metal, the base metal itself yields and the strength of the joint is governed by the mechanical properties of the base metal. In such a case the analysis does not apply. The foregoing analysis applies only when the calculated strength is less than or equal to the yield strength of the base metal.

In practice, however, the yield stress distribution across the weld zone is better approximated by a trapezoidal, than the rectangular distribution assumed above. This is due to the fact that the properties change gradually in the heat affected zone from those of the base metal to those of the cast weld metal in the fusion zone. In the fusion zone, the properties are essentially uniform. In Fig. 37, j is the width

of the central region where the yield strength is uniform and equal to σ_w.

The foregoing analysis can be applied to this central region so that

$$\sigma_b = \sigma_w \left[1 + \frac{1}{3\sqrt{3}} \cdot \frac{D}{j} \right]$$

This overestimates the actual strength of the weld, because the D/j ratio is very large, whereas the previous assumption that the weld consists only of a weld zone (having yield strength σ_w) of length h, the calculated strength is

$$\sigma_b = \sigma_w \left[1 + \frac{1}{3\sqrt{3}} \cdot \frac{D}{h} \right]$$

which underestimates the actual strength because the average yield strength of the weld zone is actually higher than σ_w.

A more realistic estimate of the strength would be given by a value of the weld zone width (of yield strength σ_w) between h and j. This may be calculated by equating the effective strength of the "constrained" region (assuming that it has a yield strength of σ_w) and the immediately adjoining "constraining" region. Hence if j + 2z is the effective width of the weld zone, then

$$\sigma_w \left[1 + \frac{1}{3\sqrt{3}} \cdot \frac{D}{j+2z} \right] = \sigma_w + \frac{(\sigma_p - \sigma_w)}{(h - j)/2} \cdot z$$

where the right hand side of the equation represents the yield strength at the section z assuming that the yield strength gradient in the heat affected zone is linear. Solving this quadratic equation yields:

$$z = -\frac{j}{4} + \left[\frac{j^2}{16} + \frac{\sigma_w D (h-j)}{12\sqrt{3}\,(\sigma_p - \sigma_w)}\right]^{1/2}$$

The strength of the joint σ_b, is then given by

$$\sigma_b = \sigma_w + \frac{2(\sigma_p - \sigma_w)}{(h-j)}\left[-\frac{j}{4} + \frac{j^2}{16} + \frac{\sigma_w D(h-j)}{12\sqrt{3}\,(\sigma_p - \sigma_w)}\right]^{1/2} \qquad \text{(II)}$$

It should be noted that this will also underestimate the strength since the actual trapezoidal yield strength distribution is approximated by a rectangular yield strength distribution across the joint. This expression would be more accurate where the slope $(\sigma_p - \sigma_w)/(h-j)/2$ in the trapezoid is very steep.

It would appear from the discussion so far that failure occurs at the interface between the weld zone and the base metal. This is not true. The initial derivation of strength based on a weld zone of uniform properties is analytically sound but the actual weld does not conform to the assumptions accurately.

The effective-width analysis is a more realistic assumption for calculating the strength of the weld but does not define the state of stress in the joint. The portion of the weld zone closest to the parent metal is the strongest; failure occurs in the weakest region which is the middle of the junction. Only when the strength of the weld metal and heat affected zone is greater than or equal to the yield strength of the base metal, will the base metal flow and failure occur at some other location.

If the yield strength distribution across the weld is approximated by a triangular pattern instead of a trapezoidal pattern, the strength

of the joint can be calculated by substituting j = 0 in Eq. (II), which gives

$$\sigma_b = \sigma_w + \left[\frac{(\sigma_p - \sigma_w)\,\sigma_w}{3\sqrt{3}}\right]^{1/2} \cdot \left[\frac{D}{h}\right]^{1/2} . \qquad \text{(III)}$$

The strength of the joint is a linear function of $[D/h]^{1/2}$. Equation (I) on the other hand shows that for a rectangular yield strength distribution the strength is a linear function of D/h.

These same general conclusions hold for a trapezoidal yield strength distribution across the joint.

A similar analysis (ignoring strength gradient) on welds made in plates under the assumption of plane strain yields (see Appendix)

$$\sigma_b = \frac{2\,\sigma_w}{\sqrt{3}}\left[1 + \frac{t}{4h}\right] \qquad \text{(IV)}$$

where t is the thickness of the plate.

Based on a similar reasoning the strength of the joint for a trapezoidal yield strength distribution across the joint can be determined.

The effective width of the weld zone as before is given by solving for z in the equation

$$\sigma_w + \frac{2(\sigma_p - \sigma_w)}{(h-j)} \cdot z = \frac{2}{\sqrt{3}}\,\sigma_w\left[1 + \frac{t}{4(j+2z)}\right]$$

Simplifying

$$\left[\frac{8\sqrt{3}\,(\sigma_p - \sigma_w)}{\sigma_w\,(h-j)}\right] z^2 + \left[\frac{4\sqrt{3}\,(\sigma_p - \sigma_w)j}{\sigma_w\,(h-j)} + 4(\sqrt{3} - 2)\right] z$$

$$+ \;[2(\sqrt{3}-2)j - t] = 0 \qquad \text{(V)}$$

This equation can be solved for z.

If J = 0 (i.e. for a triangular yield strength distribution across the joint) the above equation becomes

$$\left[\frac{8\sqrt{3}\,(\sigma_p-\sigma_w)}{\sigma_w h}\right] z^2 + \left[4(\sqrt{3}-2)\right] z - t = 0$$

which gives

$$z = \frac{-(4\sqrt{3}-8) \pm \sqrt{(4\sqrt{3}-8)^2 + \frac{32\sqrt{3}.t\,(\sigma_p-\sigma_w)}{\sigma_w(h-j)}}}{\frac{16\sqrt{3}\,(\sigma_p-\sigma_w)}{\sigma_w(h-j)}} \qquad \text{(VI)}$$

The same general conclusions derived for joints in circular members can also be made for rectangular members.

Correlation of Results and Theoretical Model

Welds in circular bars were made by friction welding and in sheets by TIG and electron beam welding. Microhardness traverse was made across the center of the joint. Joints made under similar conditions were tested in tension. An approximate trapezoid was superimposed on the microhardness traverse. It should be noted that the graph of microhardness vs yield strength, Fig. 6 is not accurate in the vicinity of the recrystallization temperature. Therefore it was not possible to precisely determine the actual yield strength distribution in this region. The computations are based on the yield strengths of the base metal, and weld metal, assuming linear yield strength gradient in the heat affected zone.

As mentioned earlier, although the experiments were not designed originally to test the analytical model, the results obtained show good conformance to the model as shown in Table II. The table

compares the values of σ_b based on the simple rectangular yield strength distribution and trapezoidal yield strength distribution. All the calculated values are below the actual strength values. When the weld zone is very narrow there is a relatively small difference between the strengths based on the two yield strength distributions assumed.

The relatively large error (14.3%) in specimen No. 3 in Table II is attributed to the comparatively large heat affected zone. The analysis is not very accurate in such cases since the mechanical constraint imposed on the weld zone is small and large plastic deformation takes place in it.

It may be noted that electron beam welds in specimens No. 4 and 5 have approximately the same strength (141 and 146 ksi) although made in sheets of different thicknesses. The theoretical model also predicts approximately the same strength (136 and 135 ksi). This result is noteworthy from the point of view of the validity of the analysis. The theoretical model was based on an idealized joint and does not presume to permit the calculation of the exact strength of the joint; only a lower bound. However as the weld is pulled in tension, the width of the weld zone increases and the calculated strength goes down, but strain hardening in the metal compensates for this and hence the approximate analysis gives a fairly accurate estimate of the joint strength. As the soft zone becomes narrower the lower bound approaches the actual strength as shown by the experimental results.

V. SUMMARY AND CONCLUSIONS

TRIP steel was welded by three processes; (1) TIG, (2) electron beam, and (3) friction welding. The higest strength, 198 ksi was obtained by friction welding in a base metal of yield strength 207 ksi. The highest strength attained in TIG and electron beam welding was 139 and 155 ksi respectively. It was shown that the joint strength is a function of the geometry of the joint and the strength and the width of the softened zone. Since the high yield strength of TRIP steels is derived from warm work, the joint strength made under similar conditions may not be a function of the base metal yield strength as long as it is greater than the effective strength of the constrained weld.

The analysis was made to gain a better understanding of the various factors that affect the strength of the butt welded joint. Although it may not always be feasible to determine the exact yield strength distribution or microhardness across a weld, a fair estimate can be made based upon the process, the clearance between the members joined, the chemistry of the weld metal, physical dimensions of the weld and the shielding. The weld has fundamentally a cast structure. The degree of chilling depends upon the bulk of the joint and the environment and the physical and metallurgical properties of the metals being joined. The theoretical model offers an excellent basis for comparison and makes it possible to predict qualitatively the effect of change of process, process parameters, and procedures on the strength of the joint. The tests were made on joints machined smooth after welding, but in practice the built-up region (flash) may give rise to higher load carrying capacity of the joint, or may lower it due to the notch effect thereby produced.

In cases where there is very little or no plastic strain in the base metal, the welds fail in a brittle manner. In general, as the weld zone becomes narrower the strength increases but the joint becomes more brittle. However, if the weld can be made stronger than the base metal, the latter yields thus resulting in large uniform elongation. TRIP steel has about 30-35% ductility and this is of great value in structural applications. As seen thus, within the scope of this investigation, the strength depends upon the diameter (or thickness) of the weld and the width of the weld zone. Thus it may be possible to achieve 100% joint efficiency in heavier sections since the width of the weld zone may not necessarily increase proportionately. The present study was made with welds having small cross-sectional areas.

Since the yield strength of TRIP steel can be controlled within limits by proper balance of alloying element and thermomechanical treatment, sometimes it may be advantageous to reduce the yield strength of the base metal slightly in order to obtain a "ductile" weld.

APPENDIX

Welds in Bars of Circular Cross-Section

Consider that the weld is made in bars of diameter D. The width of the weld zone is "h" as shown in Fig. 36. The yield strength of the weld zone is assumed to be uniform in simple tension (σ_w) while the yield strength of the parent metal is designated σ_p.

Axisymmetric solutions can be obtained for this system subjected to tensile stresses when body and inertial stresses are ignored. Consider the wedge of Fig. 42 subjected to uniform stresses indicated. Equilibrium in the radial direction requires that

$$- \frac{\partial}{\partial r} (\sigma_r \, \delta\theta \, r) \, dr + 2\sigma_\theta \, h \, dr \quad \sin \frac{\delta\theta}{2} - 2k \, \delta\theta \, r \, dr = 0$$

where k is the yield strength of the weld zone in shear

or, $$r \frac{d\sigma_r}{dr} + \sigma_r - \sigma_\theta + \frac{2\,kr}{h} = 0$$

or, $$\frac{d\sigma_r}{dr} + \frac{\sigma_r - \sigma_\theta}{r} + \frac{2k}{h} = 0 \qquad \text{(1a)}$$

von Mises yield condition for this case to produce yielding under uniaxial tension is given by

$$\sigma_w = \frac{1}{\sqrt{2}} \sqrt{(\sigma_z - \sigma_r)^2 + (\sigma_r - \sigma_\theta)^2 + (\sigma_\theta - \sigma_z)^2}$$

Under these conditions the general state of stress is that of uniaxial tension along the z direction combined with a hydrostatic tension in the transverse direction.

Thus

$$\sigma_z = \sigma_w + \sigma_r$$

and

$$\sigma_r = \sigma_\theta \ .$$

These conditions satisfy the von Mises yield criterion and can be verified by substitution.

Hence,

$$\sigma_r - \sigma_z = \sigma_w = \sqrt{3}\ k \ .$$

The equation of equilibrium (Eq. 1a) then becomes

$$\frac{d\sigma_r}{dr} + \frac{2k}{h} = 0 \qquad (2a)$$

Also since

$$\sigma_w = \sigma_r - \sigma_z$$

and since σ_w is not a function of the radius r we have

$$\frac{d\sigma_r}{dr} = \frac{d\sigma_z}{dr}$$

Equation (2a) becomes

$$\frac{d\sigma_z}{dr} + \frac{2k}{h} = 0$$

or,

$$d\sigma_z = -\frac{2k}{h} \cdot dr$$

or,

$$\sigma_z = -\frac{2k}{h}\ r + A$$

where A is a constant of integration.

At the free surface $(r = \frac{D}{2})$, $\sigma_r = 0$ hence $\sigma_z = \sigma_w$.

Therefore,

$$\sigma_w = - \frac{2k}{h} \frac{D}{2} + A$$

or,

$$A = \sigma_w + \frac{2k}{h} \frac{D}{2}$$

which gives

$$\sigma_z = \sigma_w \left[1 + \frac{2}{h\sqrt{3}} \left(\frac{D}{2} - r \right) \right] \tag{3a}$$

From Eq. (2a) the value of σ_r can be calculated as follows

$$\frac{d\sigma_r}{dr} = - \frac{2k}{h}$$

Integrating

$$\sigma_r = - \frac{2k}{h} r + B$$

where B is a constant of integration.

At $r = \frac{D}{2}$, $\sigma_r = 0$.

Therefore,

$$B = \frac{2k}{h} \cdot \frac{D}{2}$$

which gives

$$\sigma_r = \sigma_\theta = \frac{2\,\sigma_w}{\sqrt{3}\,h} \left[\frac{D}{2} - r \right] \tag{4a}$$

From Eq. (3a) we obtain the average breaking stress σ_b of the joint as

$$\sigma_b = \frac{4}{\pi D^2} \int_0^{D/2} \sigma_z \, 2\pi r dr$$

$$= \frac{4}{\pi D^2} \left[\int_0^{D/2} \sigma_w \left\{ 1 + \frac{2}{h\sqrt{3}} \left(\frac{D}{2} - r \right) \right\} 2\pi r dr \right]$$

which gives

$$\sigma_b = \sigma_w \left[1 + \frac{1}{3\sqrt{3}} \frac{D}{h} \right] \qquad \text{I}$$

Joints Made in Plates

A similar analysis can be made for butt joints made in members of rectangular cross-section under the assumption of plane strain. Consider the segment of the weld zone of thickness dx as shown in Fig. 42. Under the assumptions that plane sections remain plane, and ignoring body and inertial forces, equilibrium in the x direction demands that

$$\sigma_x W h - 2kW\,dx - \left[\sigma_x + \frac{\partial \sigma_x}{\partial x} dx \right] Wh = 0$$

or

$$\frac{d\sigma_x}{dx} = -\frac{2k}{h} \qquad (5a)$$

von Mises yield condition gives

$$\sigma_w = \sqrt{3}k = \sqrt{\frac{1}{2}[\sigma_x - \sigma_y]^2 + [\sigma_y - \sigma_z]^2 + [\sigma_z - \sigma_x]^2}$$

and

$$\sigma_y = \frac{\sigma_z + \sigma_x}{2}$$

Therefore,

$$\sigma_w = \sqrt{\frac{3}{4}(\sigma_x - \sigma_z)^2}$$

or,

$$\sigma_z = \sigma_x - \frac{2}{\sqrt{3}} \sigma_w \quad .$$

Assuming that σ_w is not a function of x

$$\frac{d\sigma_z}{dx} = \frac{d\sigma_x}{dx}$$

Therefore, from the equilibrium equation, Eq. (5a) we get

$$d\sigma_z = -\frac{2}{h\sqrt{3}} \sigma_w \, dx \quad .$$

Integrating,

$$\sigma_z = -\frac{2}{h\sqrt{3}} \sigma_w \, x + C$$

where C is a constant of integration.

At $x = t/2$, $\sigma_x = 0$ and $\sigma_z = -\frac{2}{\sqrt{3}} \sigma_w$

Therefore,

$$C = \frac{2}{\sqrt{3}} \sigma_w \left[1 + \frac{t}{2h} \right]$$

which gives

$$\sigma_z = \frac{2}{\sqrt{3}} \sigma_w \left[1 - \frac{x}{h} + \frac{t}{2h} \right] \tag{6a}$$

From Eq. (5a) the value of σ_x can be computed as follows

$$\frac{d\sigma_x}{dx} = -\frac{2k}{h}$$

Integrating ,

$$\sigma_x = -\frac{2}{h} \frac{\sigma_w}{\sqrt{3}} x + E$$

where E is a constant of integration

At $x = \frac{t}{2}$, $\sigma_x = 0$

which gives

$$E = \frac{\sigma_w}{h\sqrt{3}} t \quad .$$

Therefore,

$$\sigma_x = \frac{\sigma_w}{h\sqrt{3}} [t - 2x] \tag{7a}$$

Average strength σ_b, required for joint failure is given by

$$\sigma_b = \frac{2}{t} \int_0^{t/2} \sigma_z \, dx$$

$$= \frac{2}{t\sqrt{3}} \sigma_w \, 2 \int_0^{t/2} \left[1 + \frac{t}{2h} - \frac{x}{h} \right] dx \tag{IV}$$

$$= \frac{2}{\sqrt{3}} \sigma_w \left[1 + \frac{t}{4h} \right]$$

REFERENCES

1. V. F. Zackay, E. R. Parker, D. Fahr, R. Busch, The Enhancement of Ductility in High-Strength Steels, ASM Trans. Quart. 60, 252 (1967).

2. A. J. McEvily, Jr., R. H. Busch, An Investigation of the Notch-Impact Strength of an Ausformed Steel, ASM Trans. Quart. 55, 654 (1962).

3. W. W. Gerberich, C. F. Martin, and V. F. Zackay, Serrated Stress-Strain Curves of Metastable Austenite in Alloy Steels, ASM Trans. Quart. 58, 85 (1965).

4. G. Thomas, D. Schmatz, and W. Gerberich, Structure and Strength of Some Ausformed Steels in High Strength Materials, John Wiley and Sons, Inc., (1965), p. 251.

5. Dieter Fahr, Strengthening Mechanisms of Ultra-High-Strength Austenitic Steel, M. S. Thesis, University of California, Berkeley. UCRL-16922, June 1966.

6. Dieter Fahr, Enhancement of Ductility in High Strength Steels, Ph. D. Thesis, University of California, Berkeley. UCRL-19060, September 1969.

7. W. W. Gerberich, P. L. Hemmings, V. F. Zackay, and E. R. Parker, Interactions Between Crack Growth and Strain-Induced Transformation, UCRL-18467, September 1968.

8. W. W. Gerberich, Metastable Austenitic Steels with Ultra-High Strenght and Toughness, UCRL-18609, November 1968.

9. N. Bredzs, Investigation of Factors Determining the Tensile Strength of Brazed Joints, Supplement to the Welding Journal, November 1954, 545-S.

ACKNOWLEDGEMENTS

The author wishes to express his grateful appreciation to Professor T. H. Hazlett of the Department of Mechanical Engineering, University of California, Berkeley for his encouragement and valuable guidance throughout the course of this investigation. Thanks are also due to Professor V. F. Zackay and W. W. Gerberich of the department of Material Science and Engineering, University of California, Berkeley for their many helpful discussions and support.

A special thanks is extended to Mrs. Gloria Pelatowski for her help in preparing the art work and to Mrs. Shirley Ashley for her patience and endurance in typing the manuscript.

This work was performed under the auspices of the U. S. Atomic Energy Commission through the Inorganic Materials Research Division of the Lawrence Radiation Laboratory, Berkeley.

Table I. Friction welding data.

No.	Diameter (in.)	Speed RPM	Upset (in.)	Weld pressure (ksi)	Forge pressure (ksi)	Forge time (sec)	Revolutions to stop	Diameter at Tension test (in.)	Ultimate tensile stress(ksi)	Remarks
1	0.250	2000	0.030	15	70	4	82	0.236	154	Voids at interface
2	0.250	2100	0.030	20	70	4	52	0.223	174	Sound bond
3	0.250	2500	0.030	40	70	4	24	0.225	177	Sound bond no yielding in base metal
4	0.250	1500	0.030	60	70	4	20	0.235	185	No yielding in base metal
5	0.250	2000	0.030	60	70	4	24	0.220	198	Yielding in base metal
6	0.250	2500	0.030	60	70	4	26	0.200	193	No yielding in base metal

Table II. Correlation of results and theoretical model

No.*	Figs.	σ_p (ksi)	h (in.)	j (in.)	D or t† (in.)	σ_w (ksi)	σ_b actual (ksi)	σ_b based on rectangular Y.S. distribution		σ_b based on trapezoidal Y.S. distribution	
								psi	error %	psi	error %
1	19,20	207	0.066	0.033	0.217	112	198	183	7.6	191	3.5
2	38,39	207	0.065	0.025	0.200	112	193	178	8.5	183	5.2
3	17,18	207	0.125	0.045	0.225	90	174	121	30.5	150	14.3
4	40,41	225	0.100	0.040	0.125	80	141	121	14.2	136	3.6
5	11,12	225	0.075	0.00	0.063	75	146	104	28.8	135	7.5

*Nos. 1, 2, and 3 are welds in round specimens and Nos. 4 and 5 are welds in sheet specimens.

†D is for Nos. 1, 2, and 3 and t for Nos. 4 and 5.

FIGURE CAPTIONS

Fig. 1. Tension specimen: sheet.

Fig. 2. Tension specimen: round.

Fig. 3. Stress-strain curve of base metal: sheet specimen.

Fig. 4. Stress-strain curve of base metal: round specimen.

Fig. 5. Variation of yield and ultimate tensile stress with maximum temperature of heating.

Fig. 6. Variation of microhardness with yield stress.

Fig. 7. Stress-strain curve: TIG weld with no filler.

Fig. 8. Microhardness traverse across TIG weld in Fig. 7.

Fig. 9. Stress-strain curve: TIG weld with maraging steel filler.

Fig. 10. Microhardness traverse across TIG weld in Fig. 9.

Fig. 11. Stress-strain curve: electron beam weld with no filler.

Fig. 12. Microhardness traverse across electron beam weld in Fig. 11.

Fig. 13. Stress-strain curve: Electron beam weld with maraging steel filler.

Fig. 14. Microhardness traverse across electron beam weld in Fig. 13.

Fig. 15. Stress-strain curve: electron beam weld with no filler tested at liquid nitrogen temperature.

Fig. 16. Friction welding specimen.

Fig. 17. Stress-strain curve: friction weld.

Speed: 2100 rpm Upset: 0.030 in.

Weld Pressure: 40 ksi Forge Pressure: 70 ksi for 4 sec.

Fig. 18. Microhardness traverse across the friction weld in Fig. 17.

Fig. 19. Stress-strain curve: friction weld.

Speed: 2000 rpm Upset: 0.030 in.

Weld pressure: 60 ksi Forge Pressure: 70 ksi for 4 sec.

Fig. 20. Microhardness traverse across the friction weld in Fig. 19.

Fig. 21. Micrograph: TRIP steel in the as rolled condition. Shows dark carbide particles. 600×

Fig. 22. Micrograph: Fusion zone in TIG weld. Shows cast cored structure, 600×.

Fig. 23. Micrograph: Boundary between fusion zone and heat affected zone in TIG weld, 600×.

Fig. 24. Micrograph: HAZ close to fusion zone in TIG weld. Shows annealing twins and local melting due to segregation during rolling, 600×.

Fig. 25. Micrograph: HAZ further away from the weld than Fig. 24. Shows excessive carbide precipitation and growth, 600×.

Fig. 26. Micrograph: Fusion zone in TIG weld with maraging steel filler. Shows area in the middle of the weld where there is more maraging steel (darker regions), 600×.

Fig. 27. Micrograph: Fusion zone adjacent to the area in Fig. 26 where there is more mixing. Shows darker maraging steel particles dispersed in austenite, 600×.

Fig. 28. Micrograph: Fusion zone in electron beam weld. Shows dendritic cored structure, 600×.

Fig. 29. Micrograph: Boundary between fusion zone and HAZ in electron beam weld. Shows grain size and annealing twins in the HAZ, 600×.

Fig. 30. Micrograph: HAZ in electron beam weld. Shows area of excessive carbide precipitation and growth, 600×

Fig. 31. Micrograph: Fusion zone in electron beam weld with maraging steel filler. Shows dark maraging steel regions dispersed in austenite, 600×.

Fig. 32. Micrograph: Friction weld interface. Shows interface from the center line of the specimen (bottom of picture) to the outer diameter (top of the picture), 95×.

Fig. 33. Micrograph: Friction weld interface close to centerline of specimens. Shows carbide precipitation, 600×.

Fig. 34. Micrograph: Friction weld interface close to outer diameter of specimen. Shows lesser concentration of carbide particles than in Fig. 33, 600×.

Fig. 35. Micrograph: HAZ in friction weld. Shows grain flow, 600×.

Fig. 36. Rectangular yield stress distribution across a butt weld.

Fig. 37. Trapezoidal yield stress distribution across a butt weld.

Fig. 38. Stress-strain curve: Friction weld. Speed: 2500 rpm. Upset: 0.030 in. Weld pressure: 60 ksi. Forge pressure: 70 ksi for 4 sec.
Data used to check theoretical model. See Table II.

Fig. 39. Microhardness traverse across the weld in Fig. 38.
Data used to check theoretical model. See Table II.

Fig. 40. Stress-strain curve: Electron beam weld with no filler.
Data used to check theoretical model. See Table II.

Fig. 41. Microhardness traverse across weld in Fig. 41.
Data used to check theoretical model. See Table II.

Fig. 42. Equilibrium of wedge element in weld zone in a round butt weld.

Fig. 43. Equilibrium of element of weld zone in a butt weld of rectangular cross section.

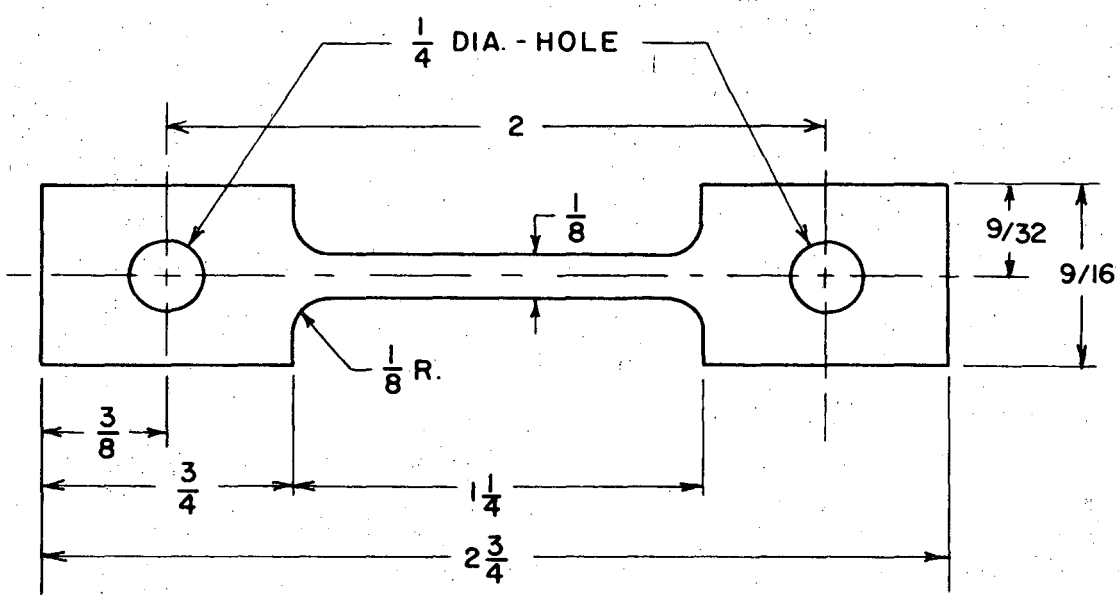

XBL 701-91

Fig. 1

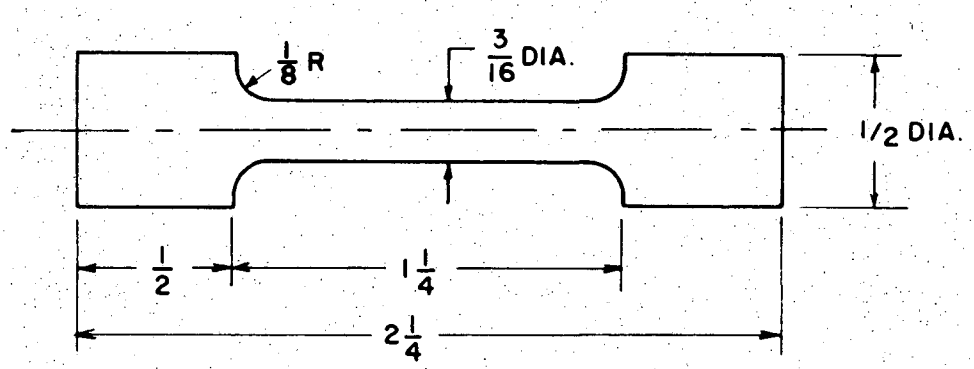

XBL 701-101

Fig. 2

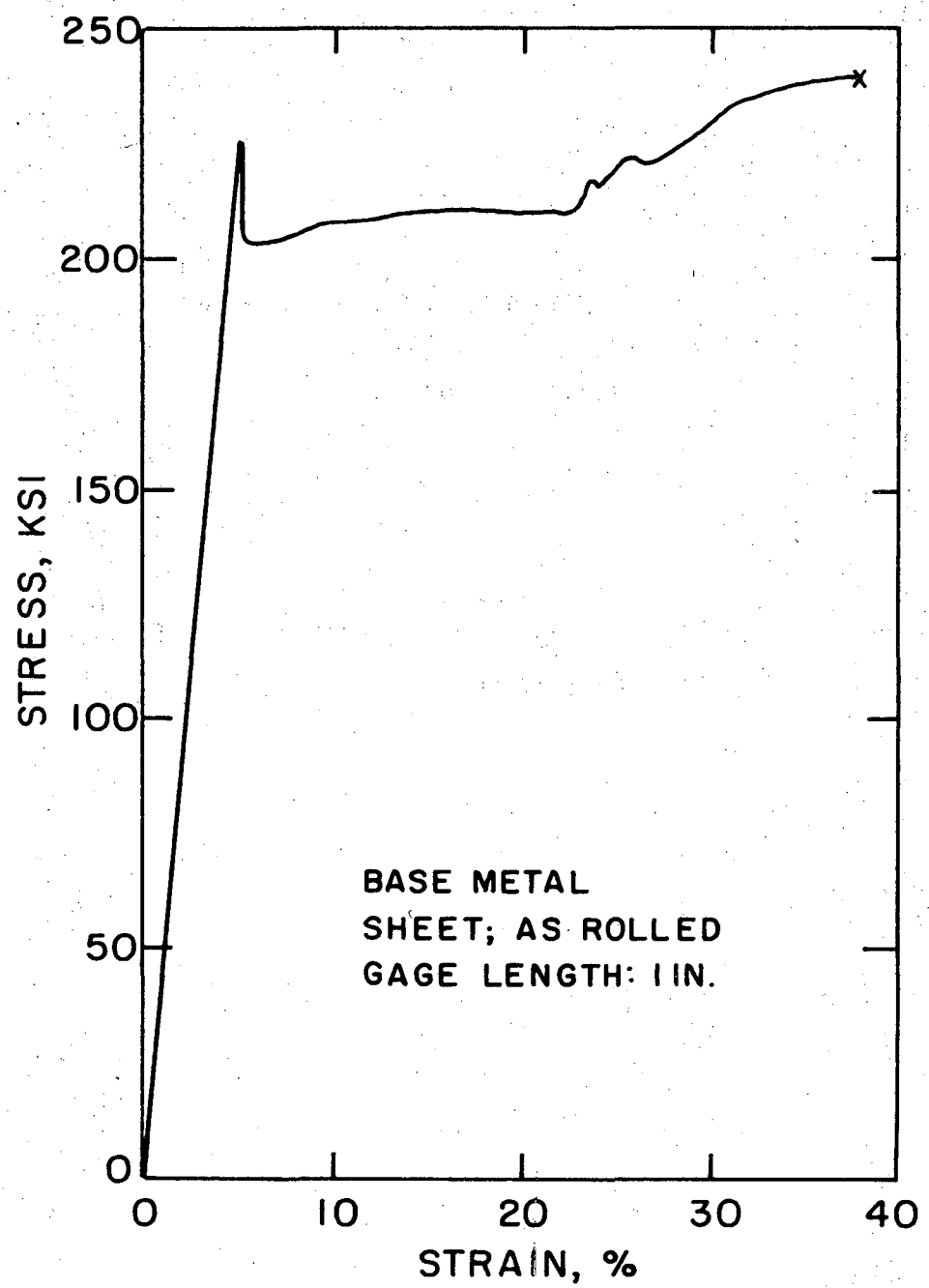

XBL 701-103

Fig. 3

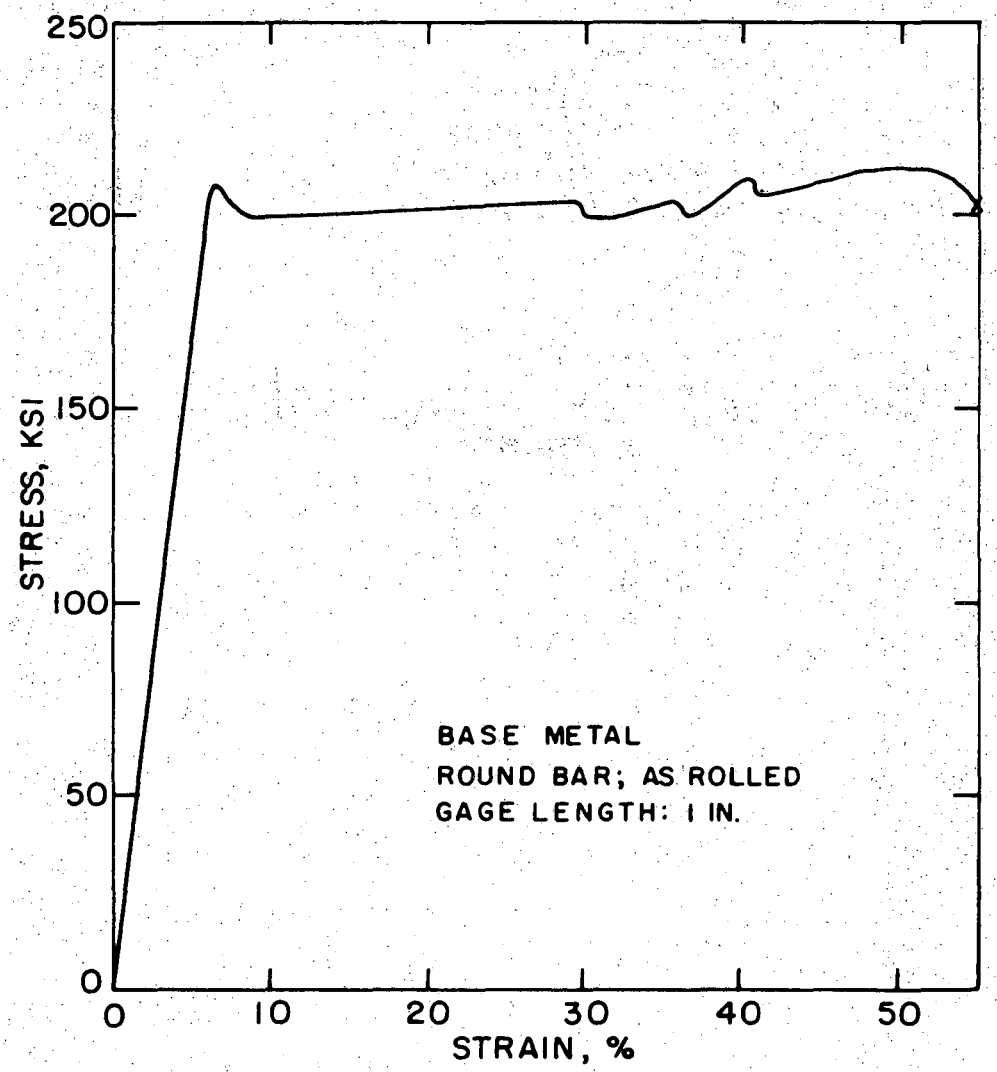

XBL 701-107

Fig. 4

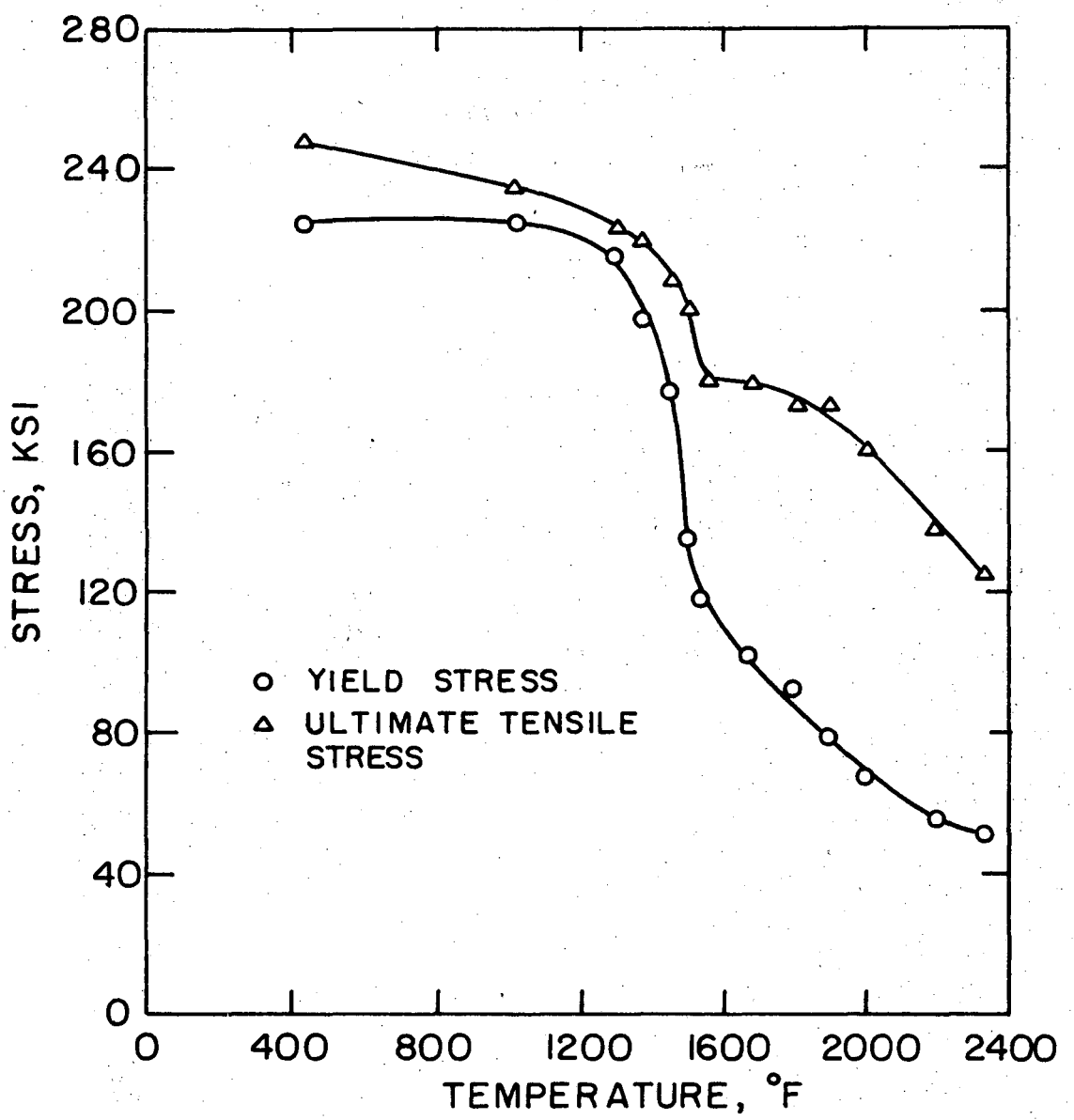

XBL 701-98

Fig. 5

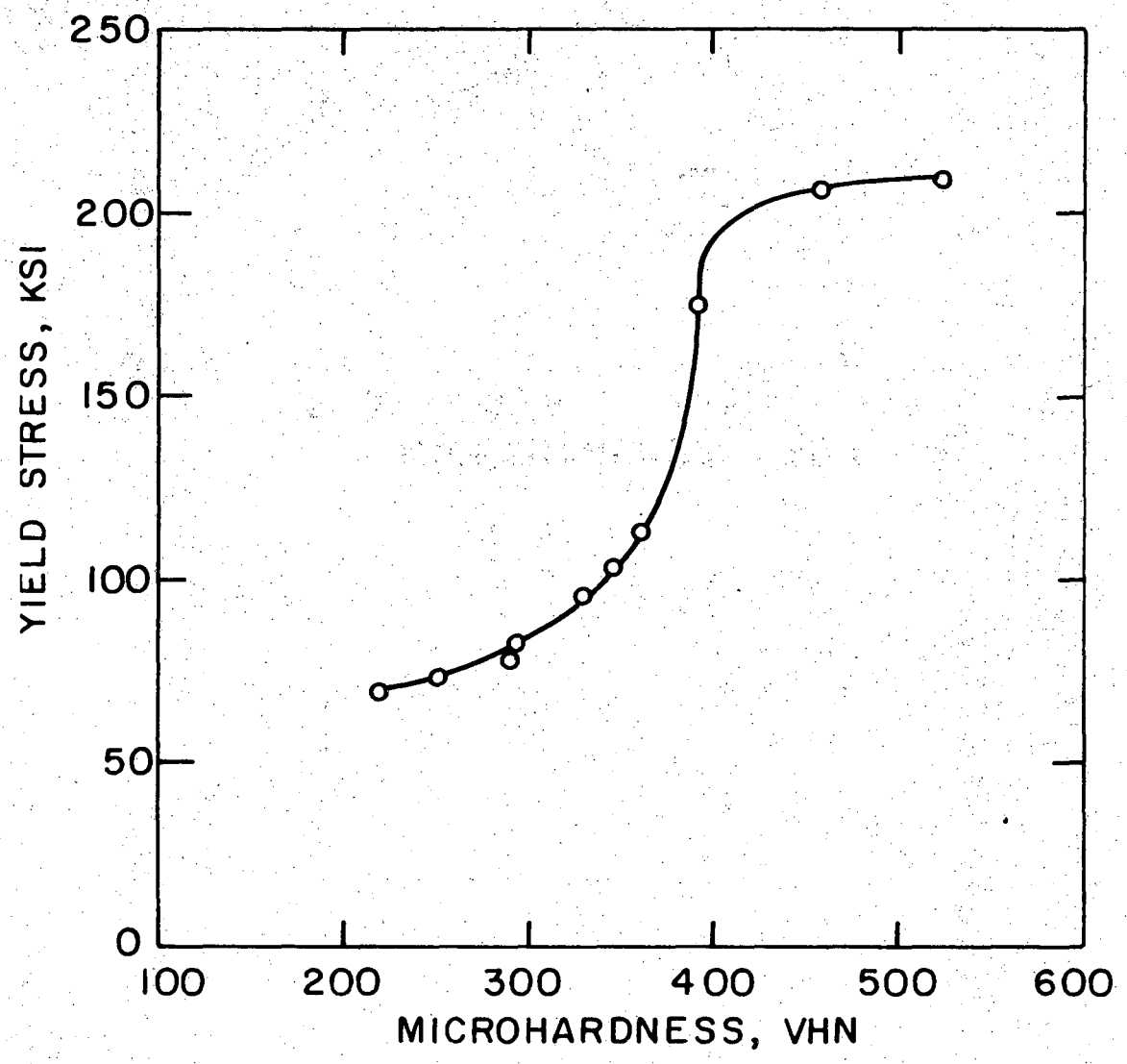

XBL 701-106

Fig. 6

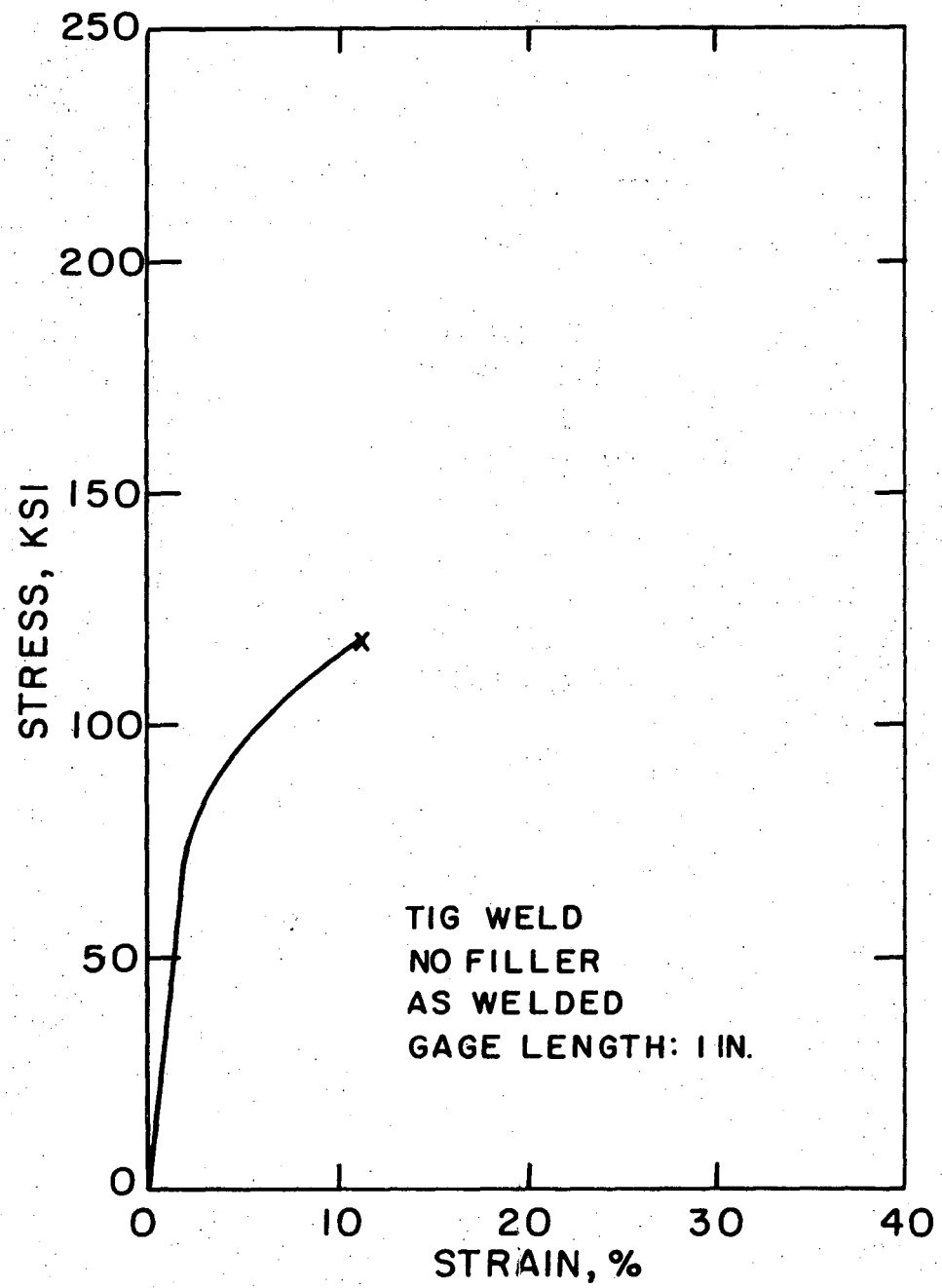

XBL 701-104

Fig. 7

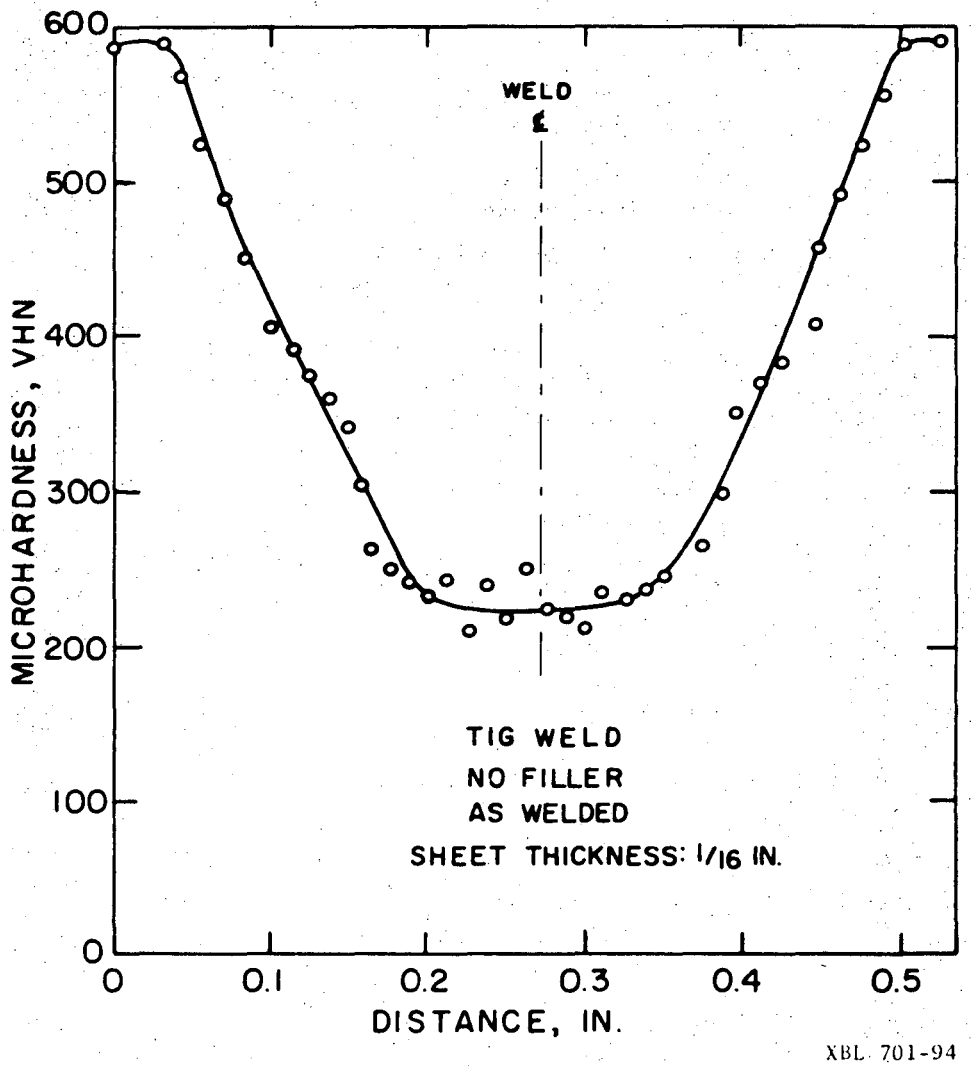
600
500
400
300
200
100
0
MICROHARDNESS, VHN
WELD
℄
TIG WELD
NO FILLER
AS WELDED
SHEET THICKNESS: 1/16 IN.
0
0.1
0.2
0.3
0.4
0.5
DISTANCE, IN.
XBL 701-94

Fig. 8

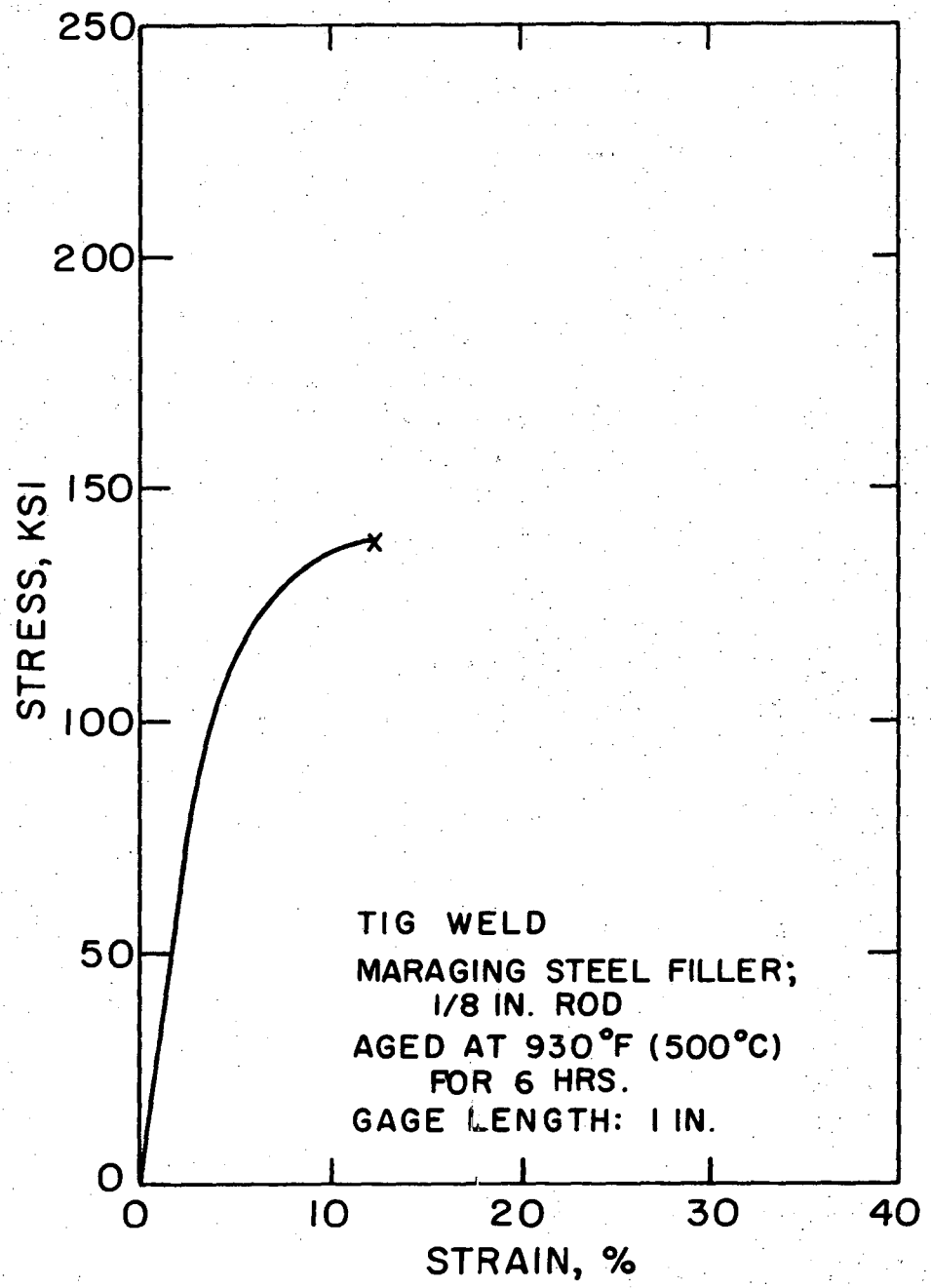

XBL 701-112

Fig. 9

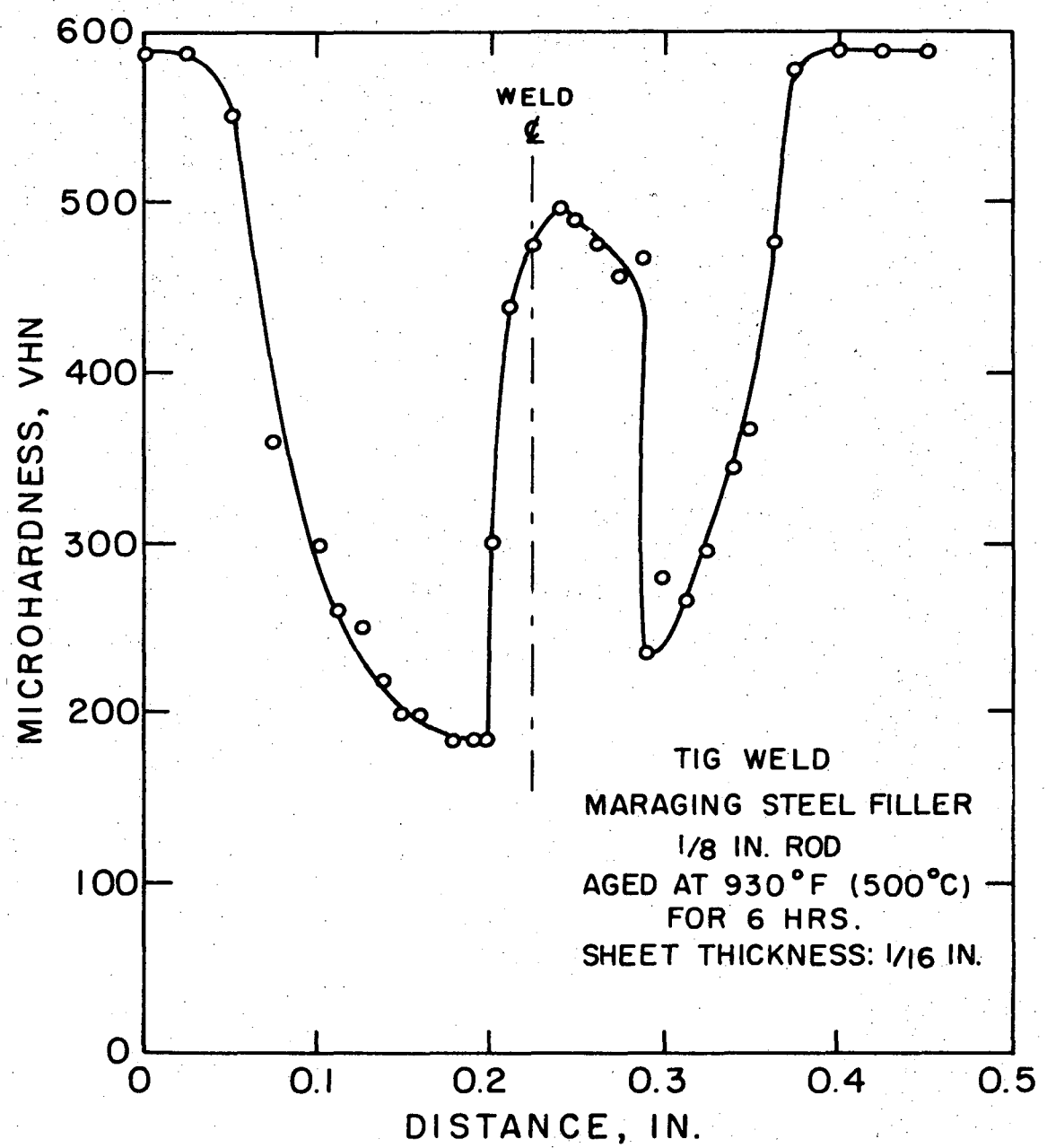

XBL 701-88

Fig. 10

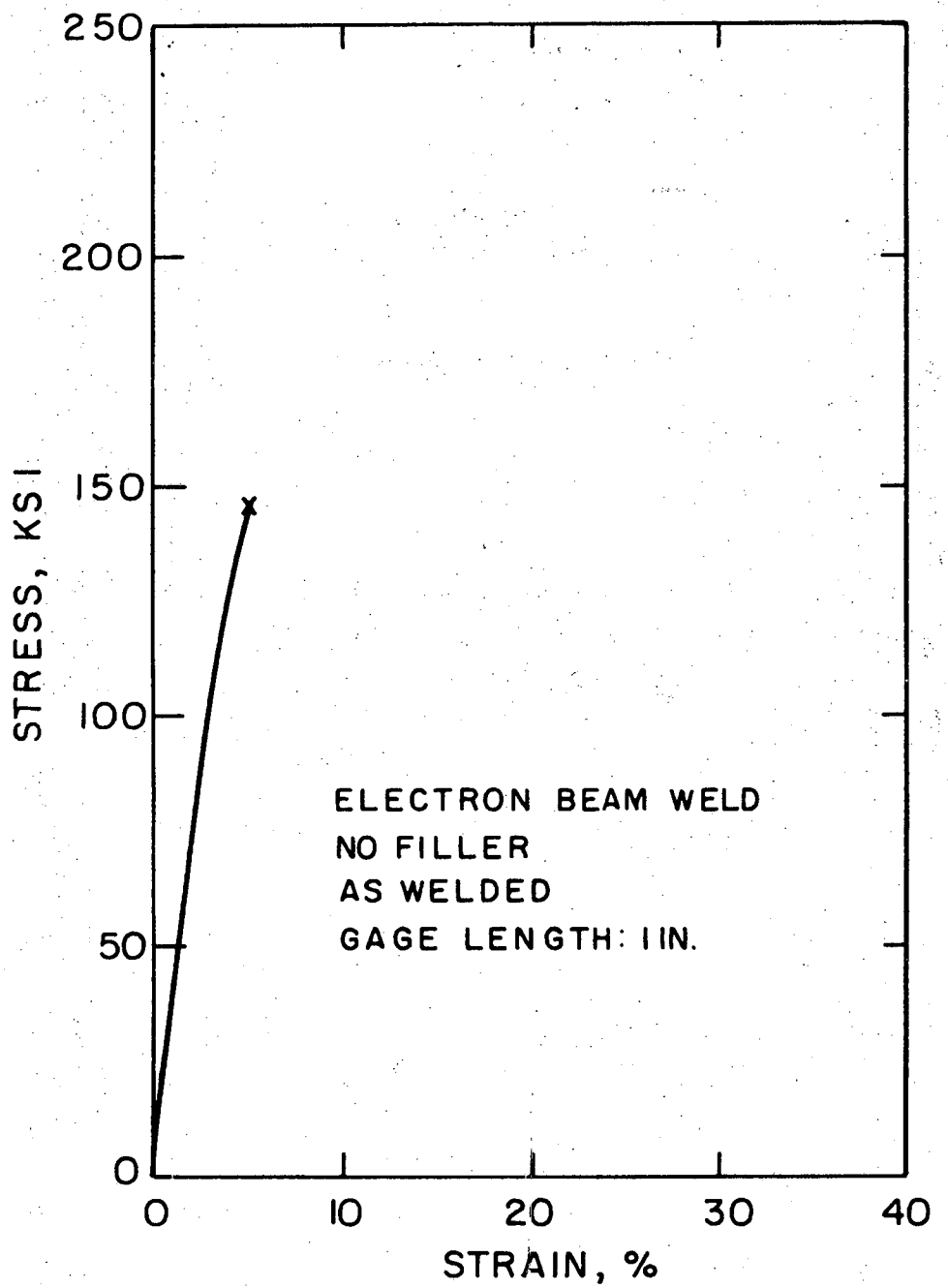

XBL 701-109

Fig. 11

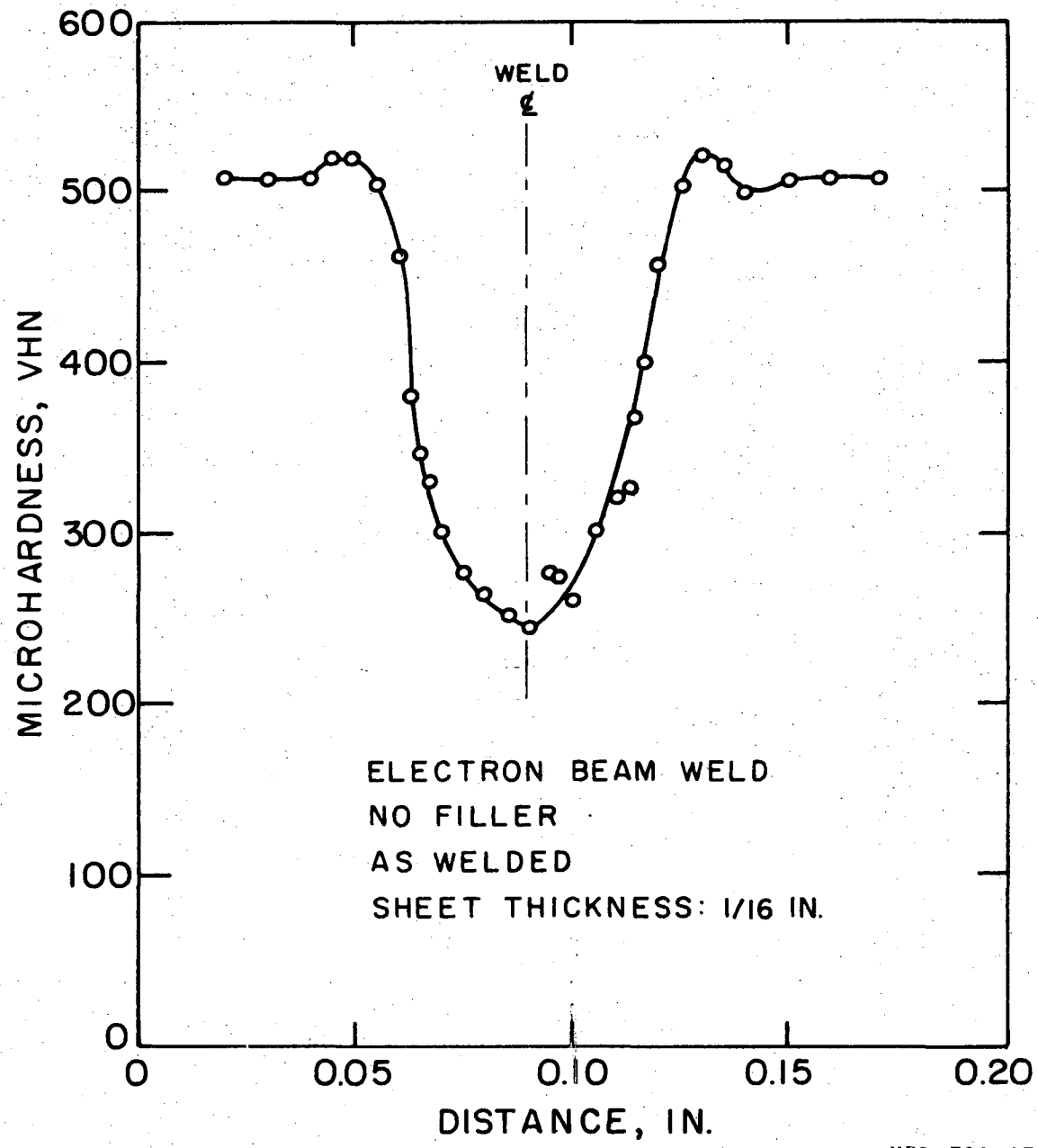

XBL 701-87

Fig. 12

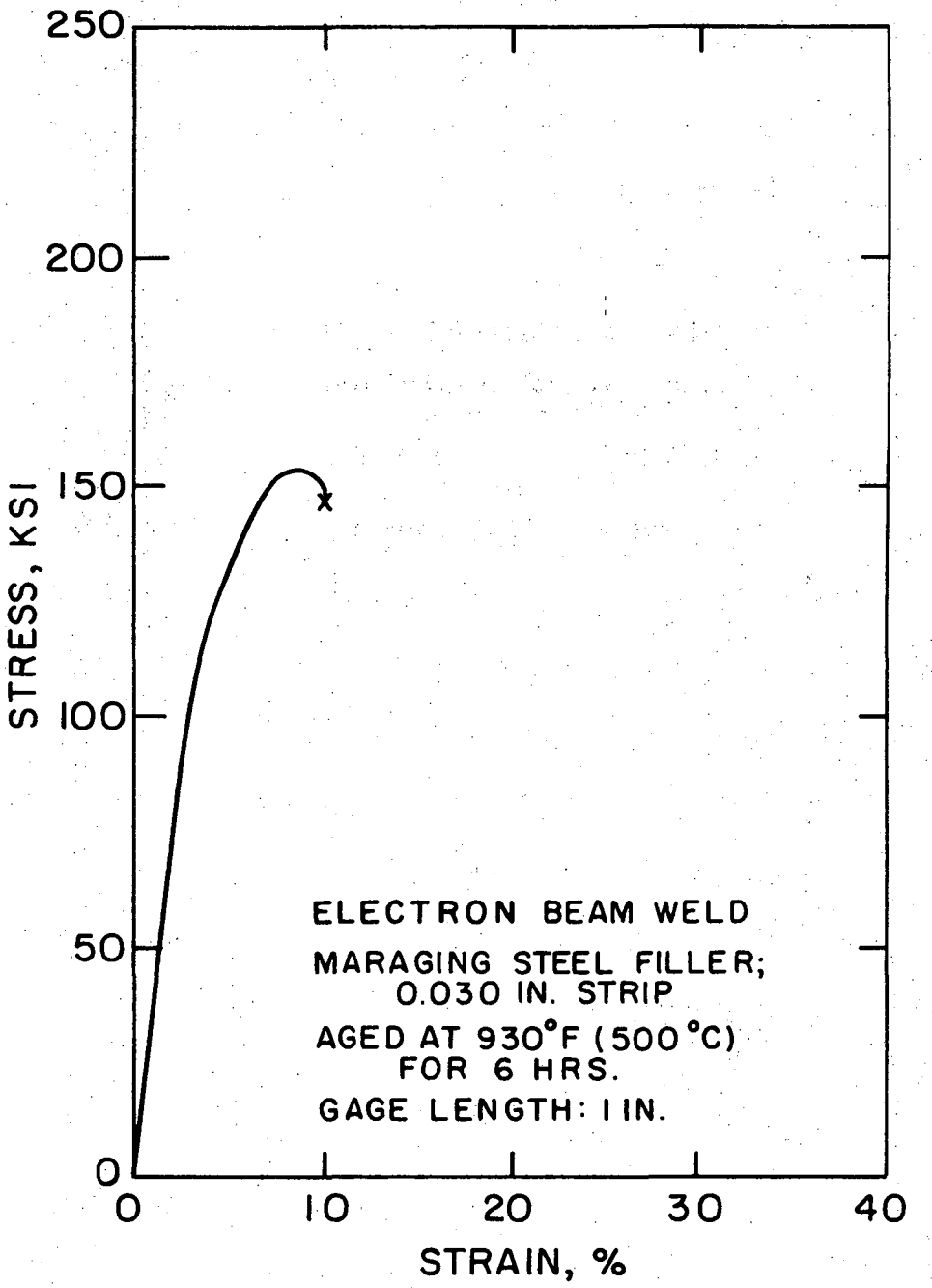

XBL 701-105

Fig. 13

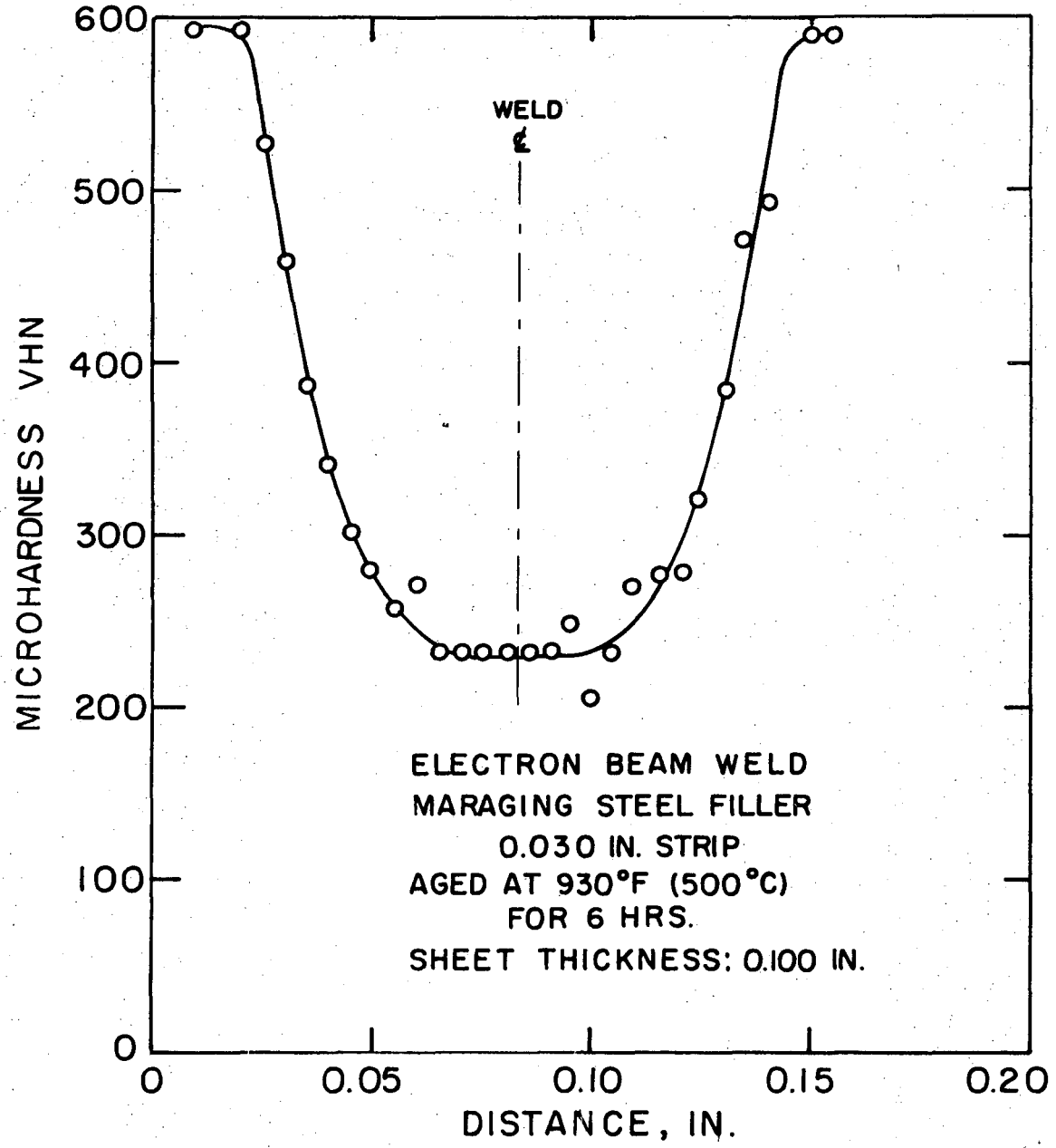

XBL 701-89

Fig. 14

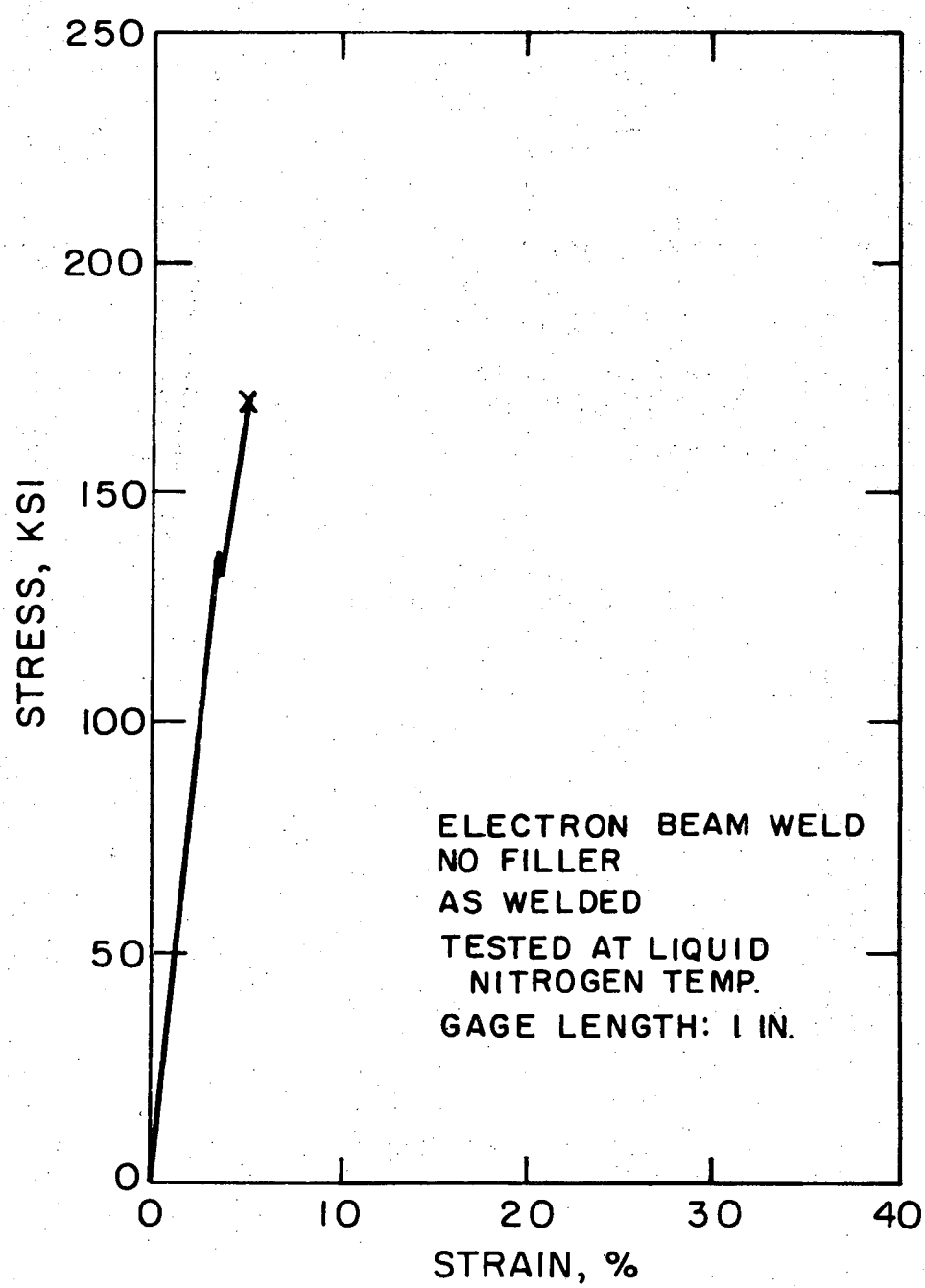

XBL 701-137

Fig. 15

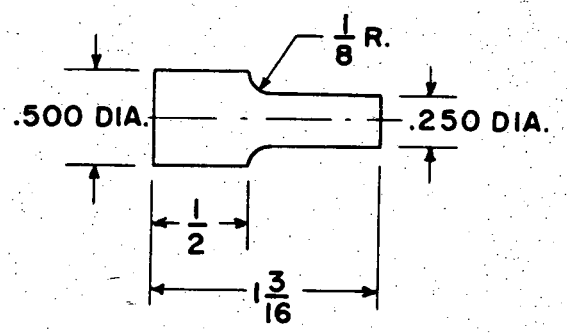

XBL 701-111

Fig. 16

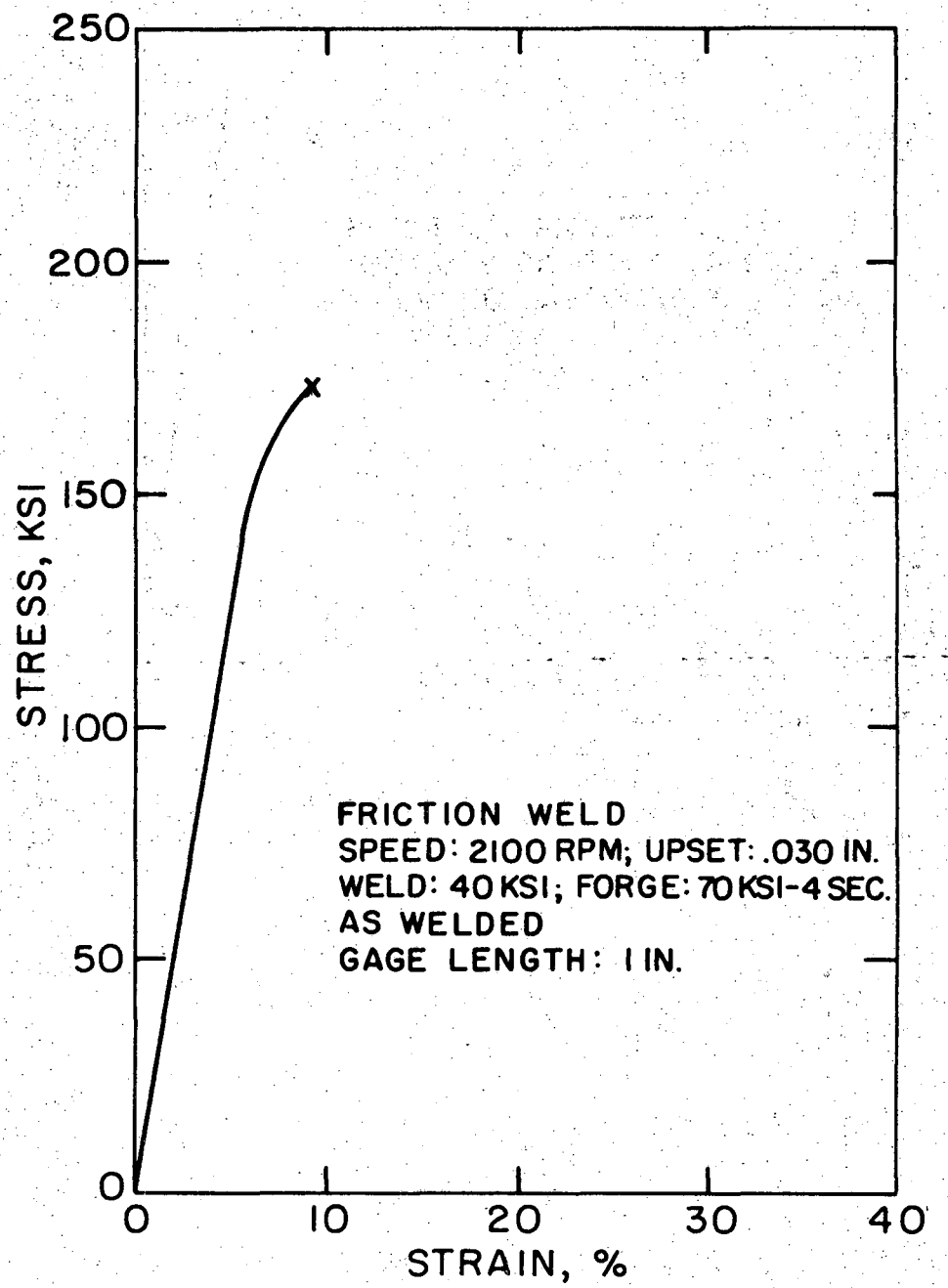

XBL 701-102

Fig. 17

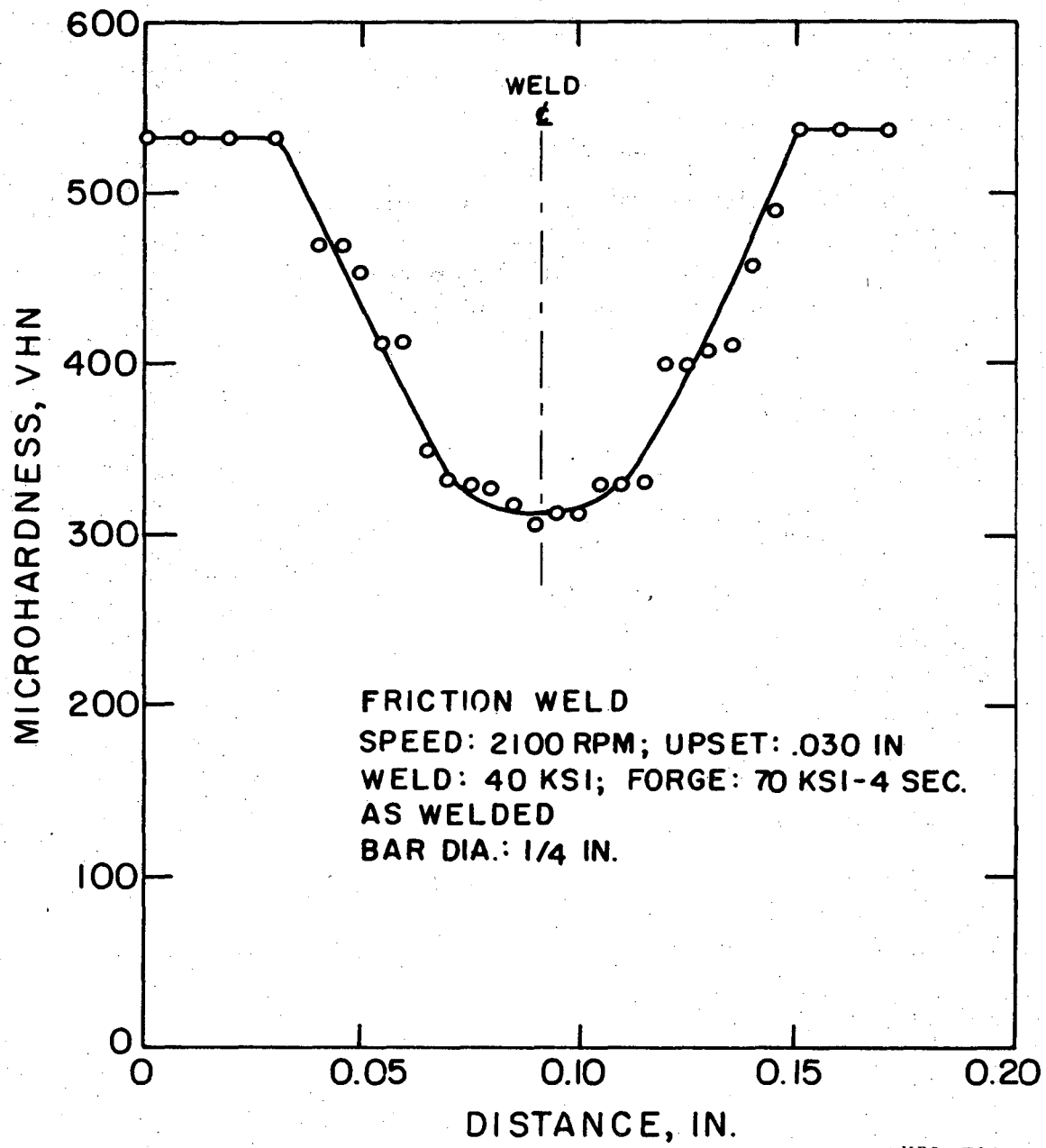

XBL 701-90

Fig. 18

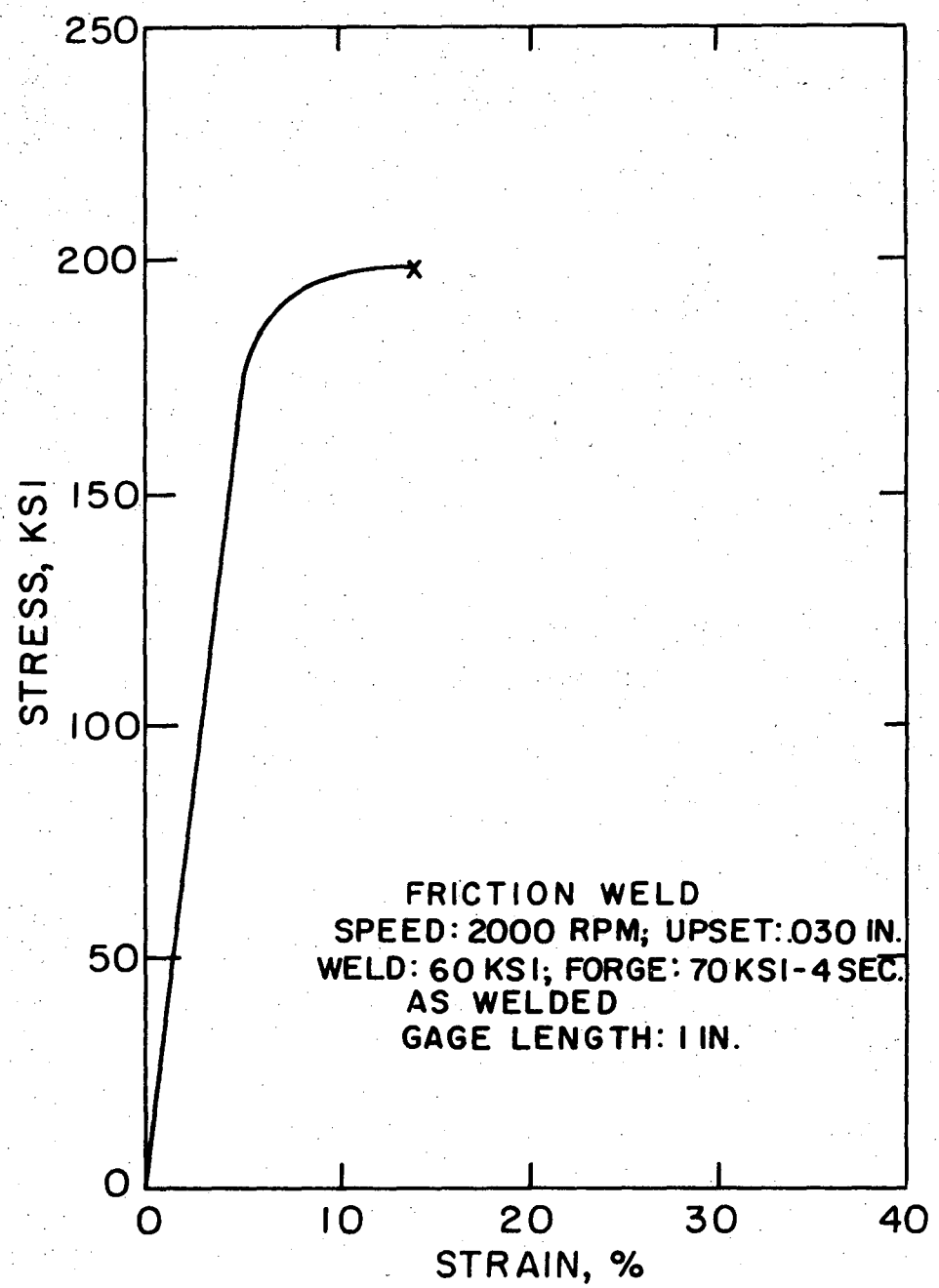

XBL 701-97

Fig. 19

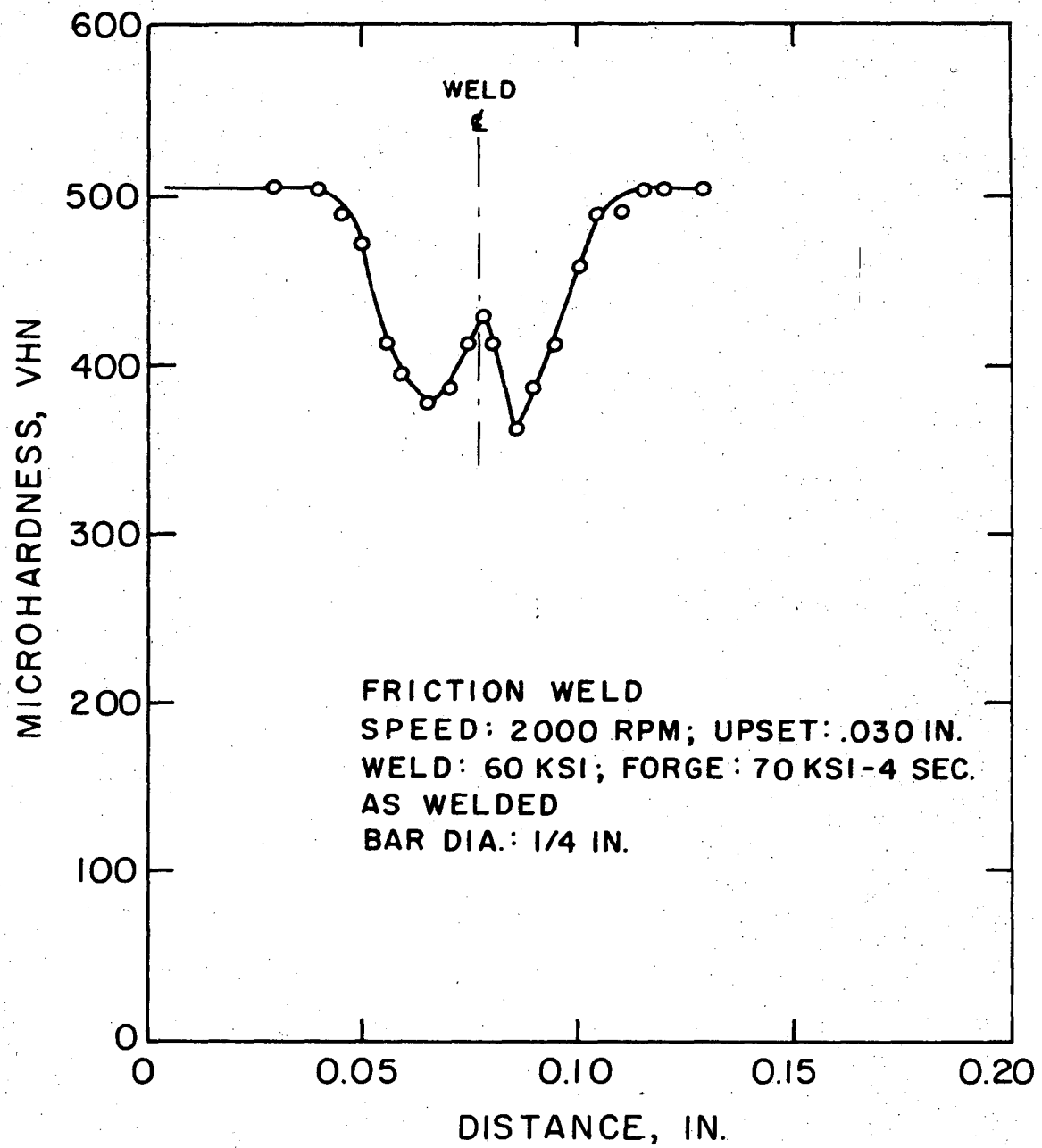

XBL 701-95

Fig. 20

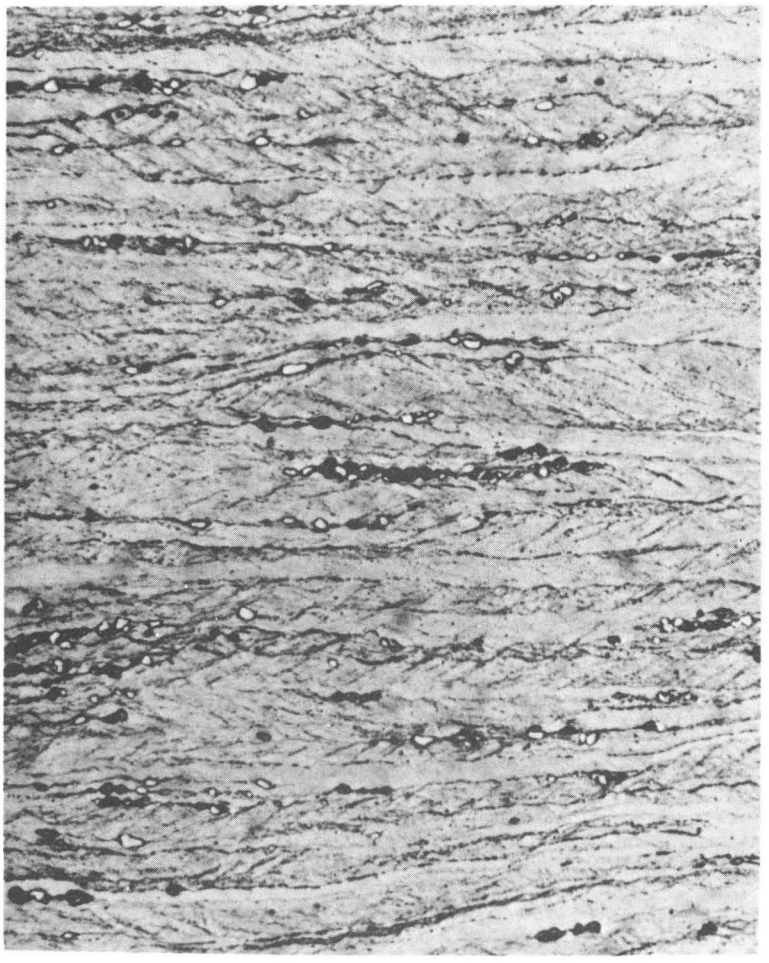

XBB 701-165

Fig. 21

XBB 701-169

Fig. 22

XBB 701-170

Fig. 23

XBB 701-171

Fig. 24

XBB 701-172

Fig. 25

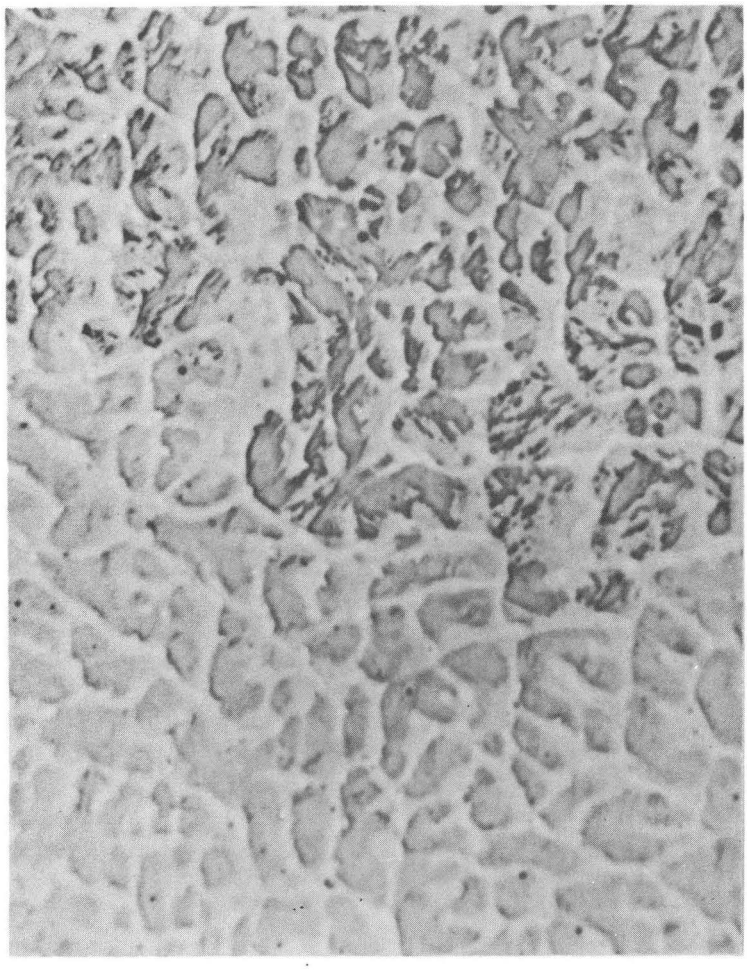

XBB 701-173

Fig. 26

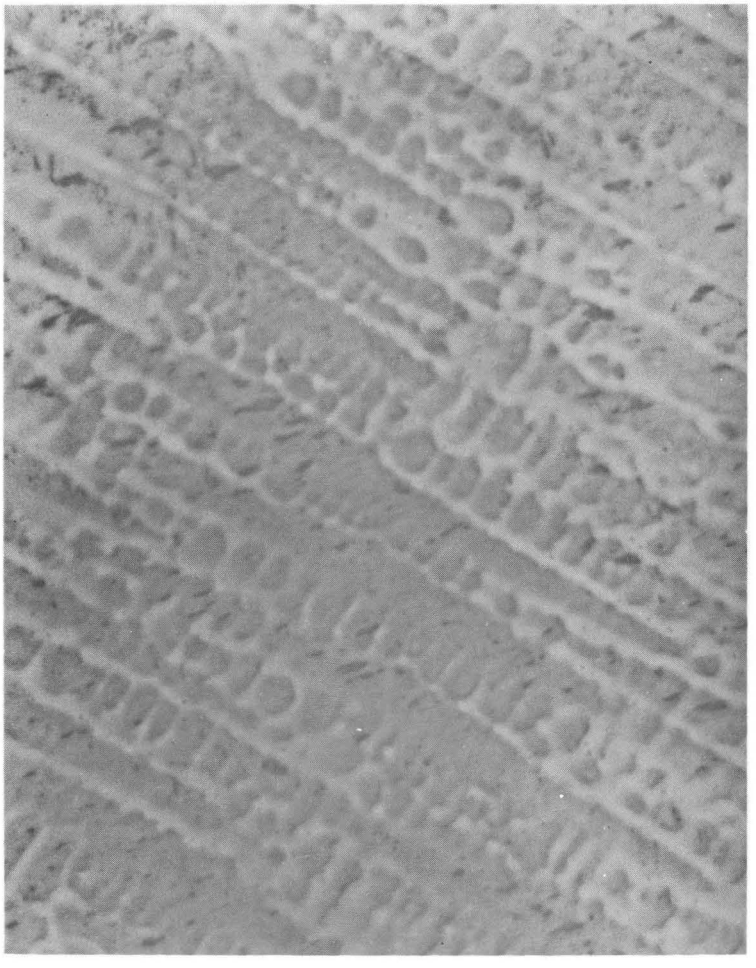

XBB 701-160

Fig. 27

XBB 701-159

Fig. 28

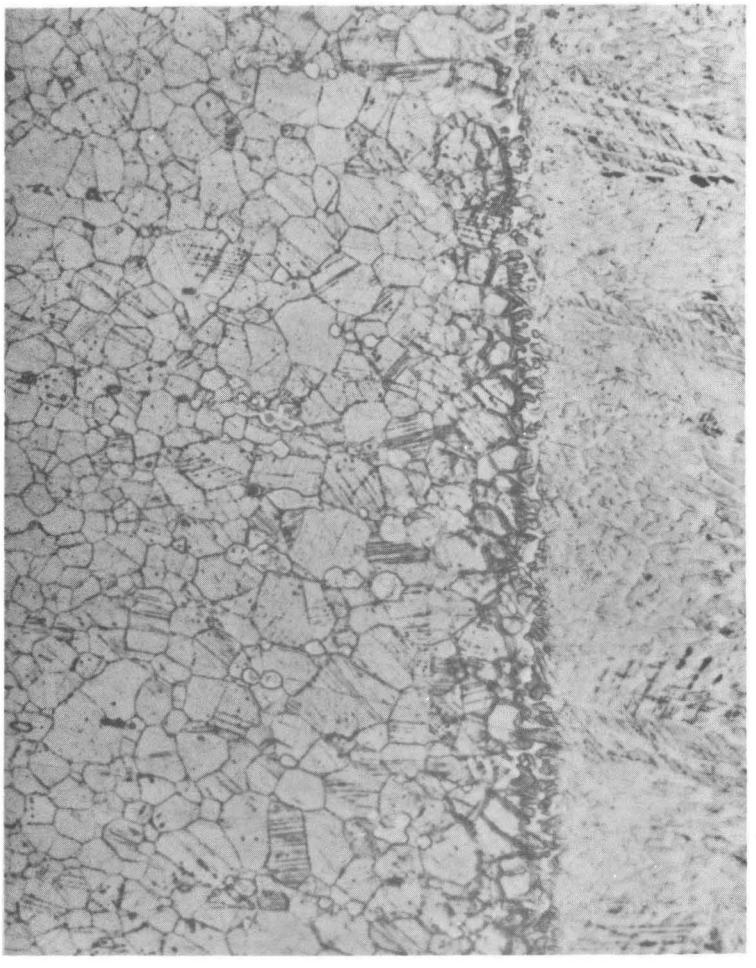

XBB 701-161

Fig. 29

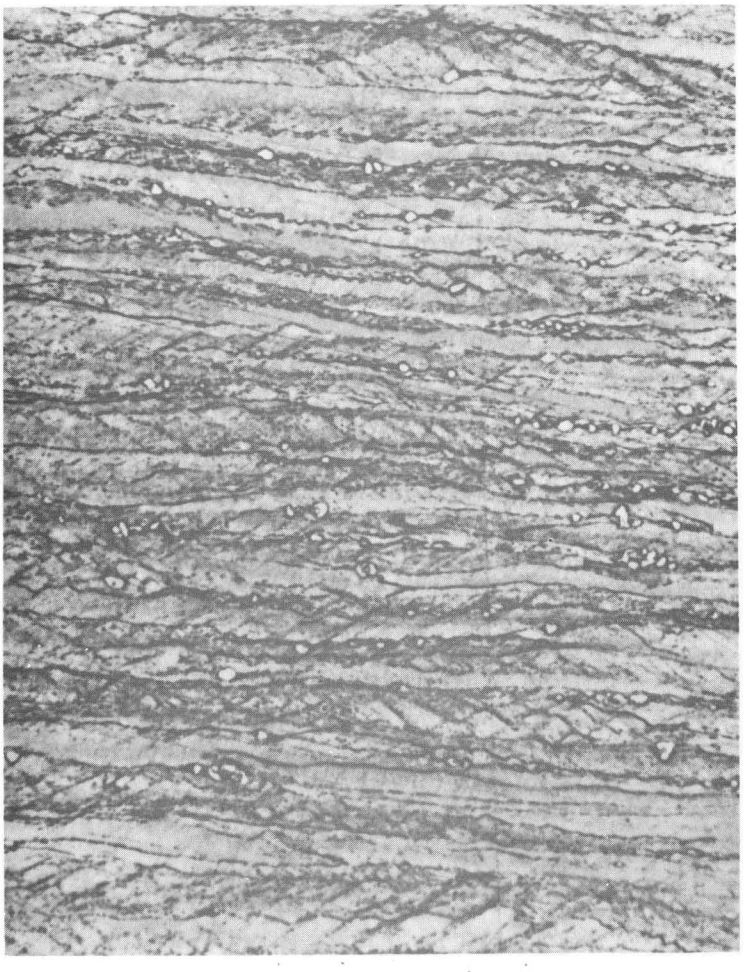

XBB 701-166

Fig. 30

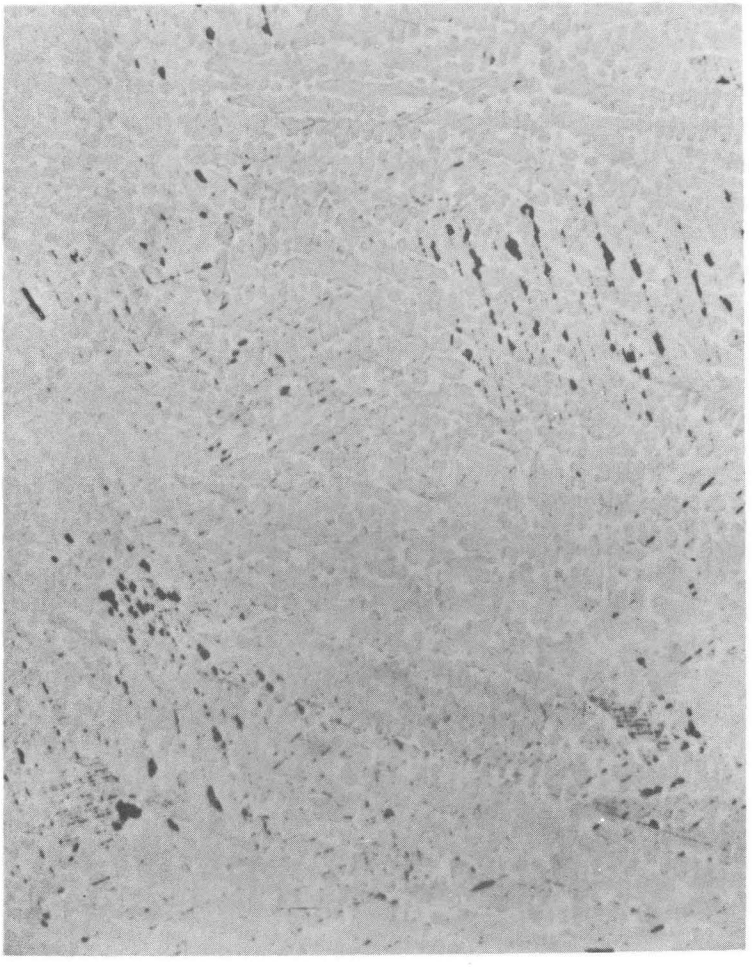

XBB 701-162

Fig. 31

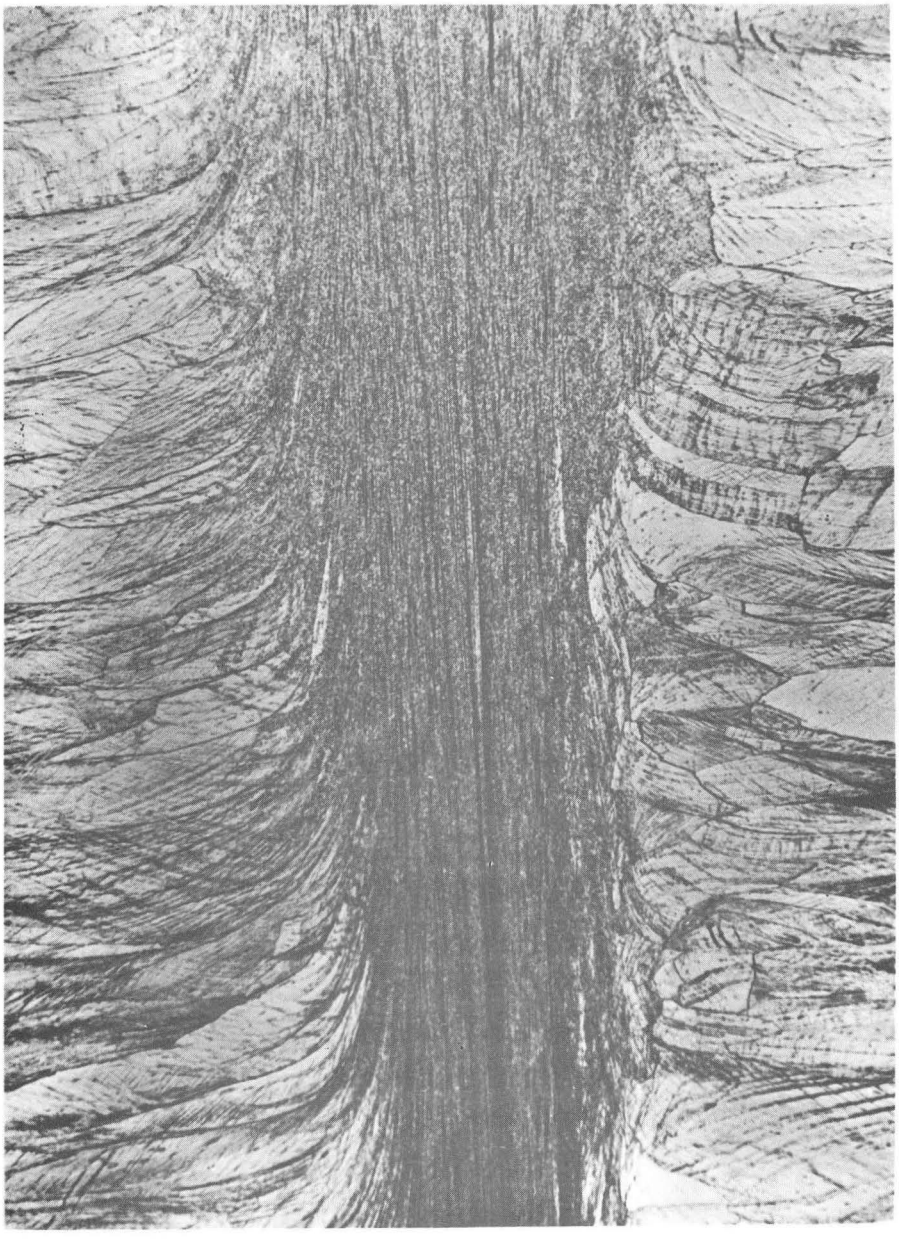

XBB 701-164

Fig. 32

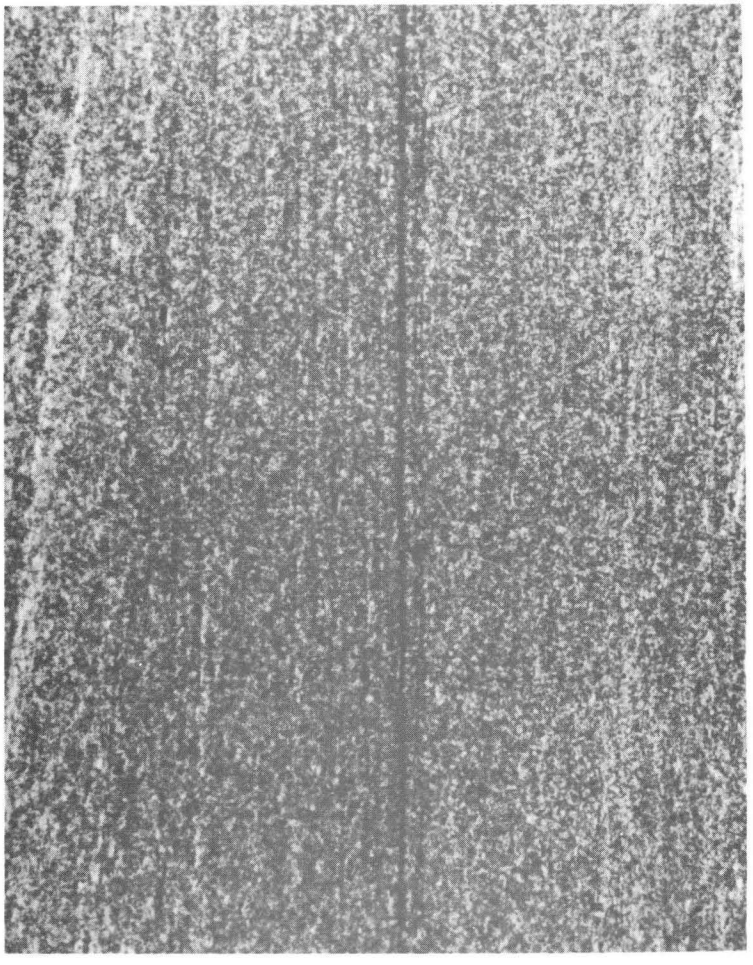

XBB 701-163

Fig. 33

XBB 701-167

Fig. 34

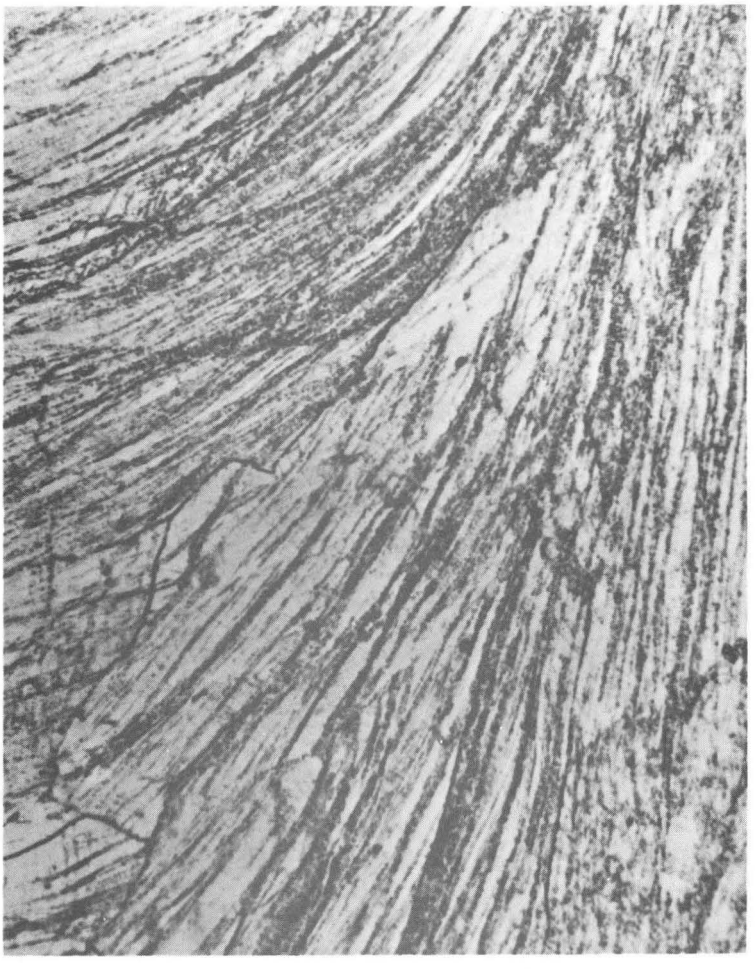

XBB 701-168

Fig. 35

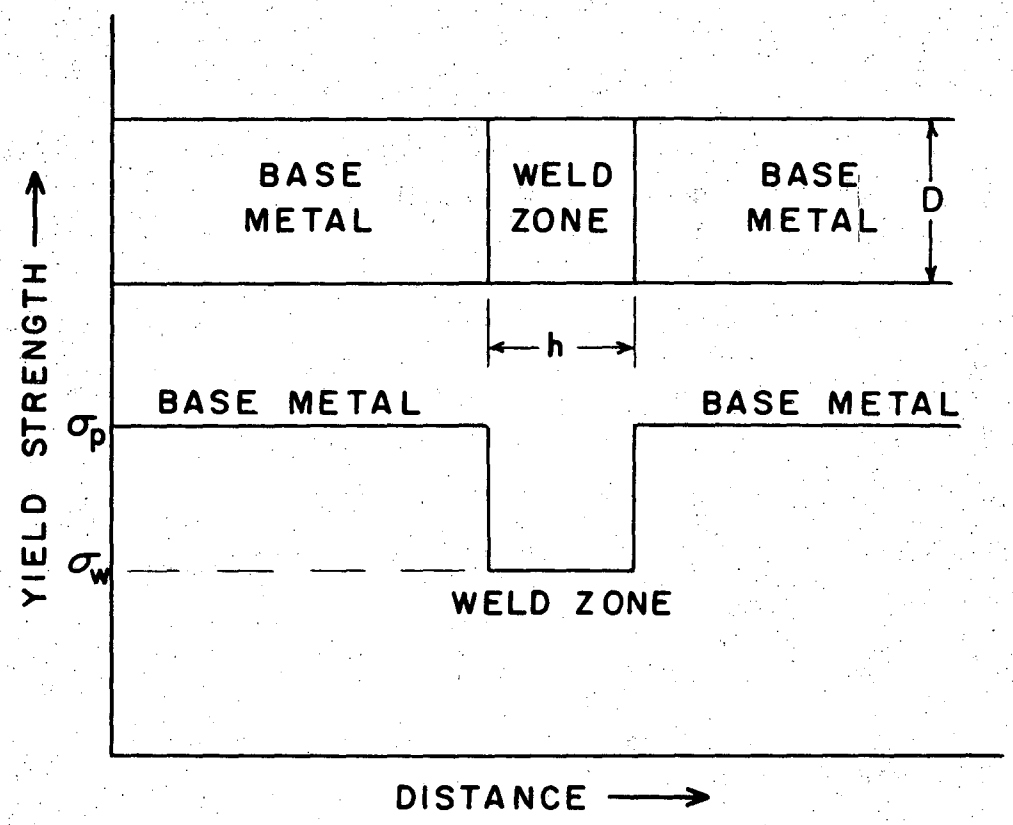

XBL 701-96

Fig. 36

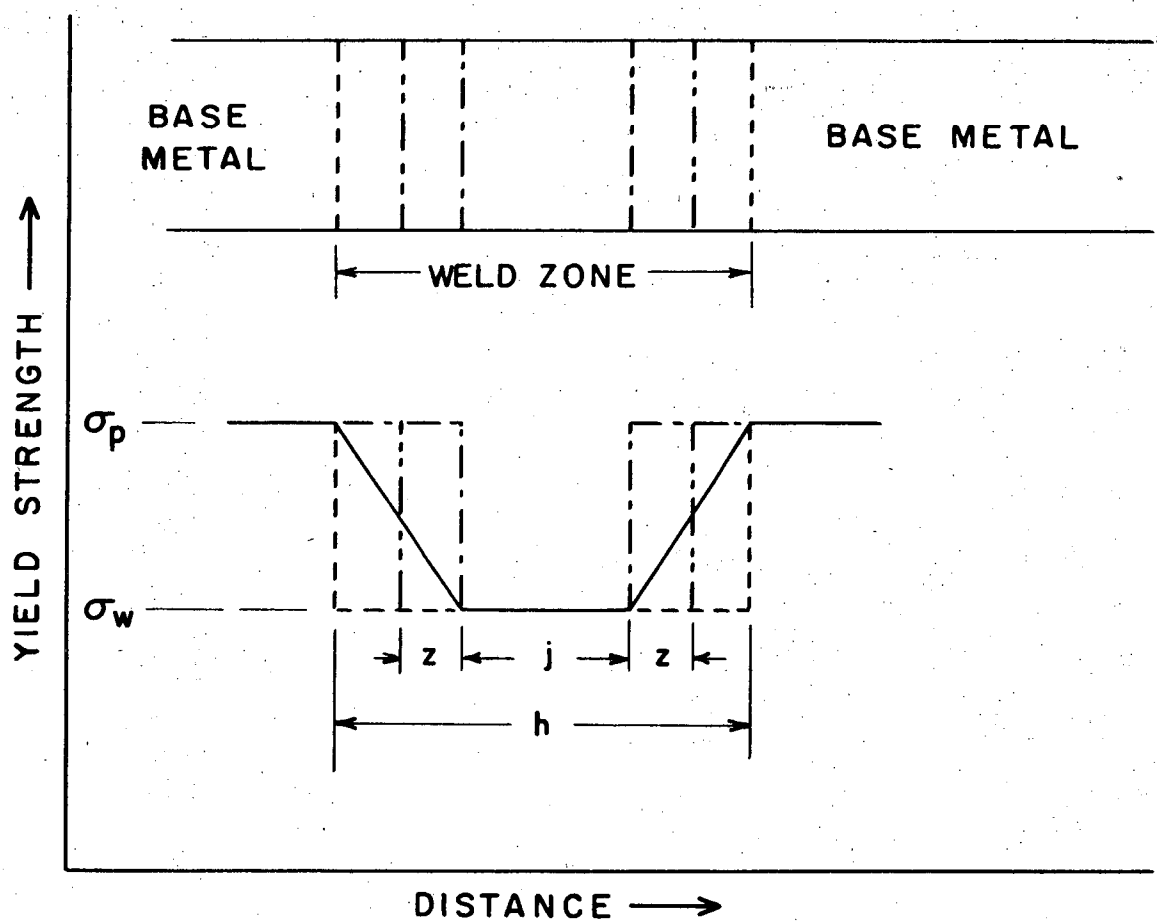

XBL 701-113

Fig. 37

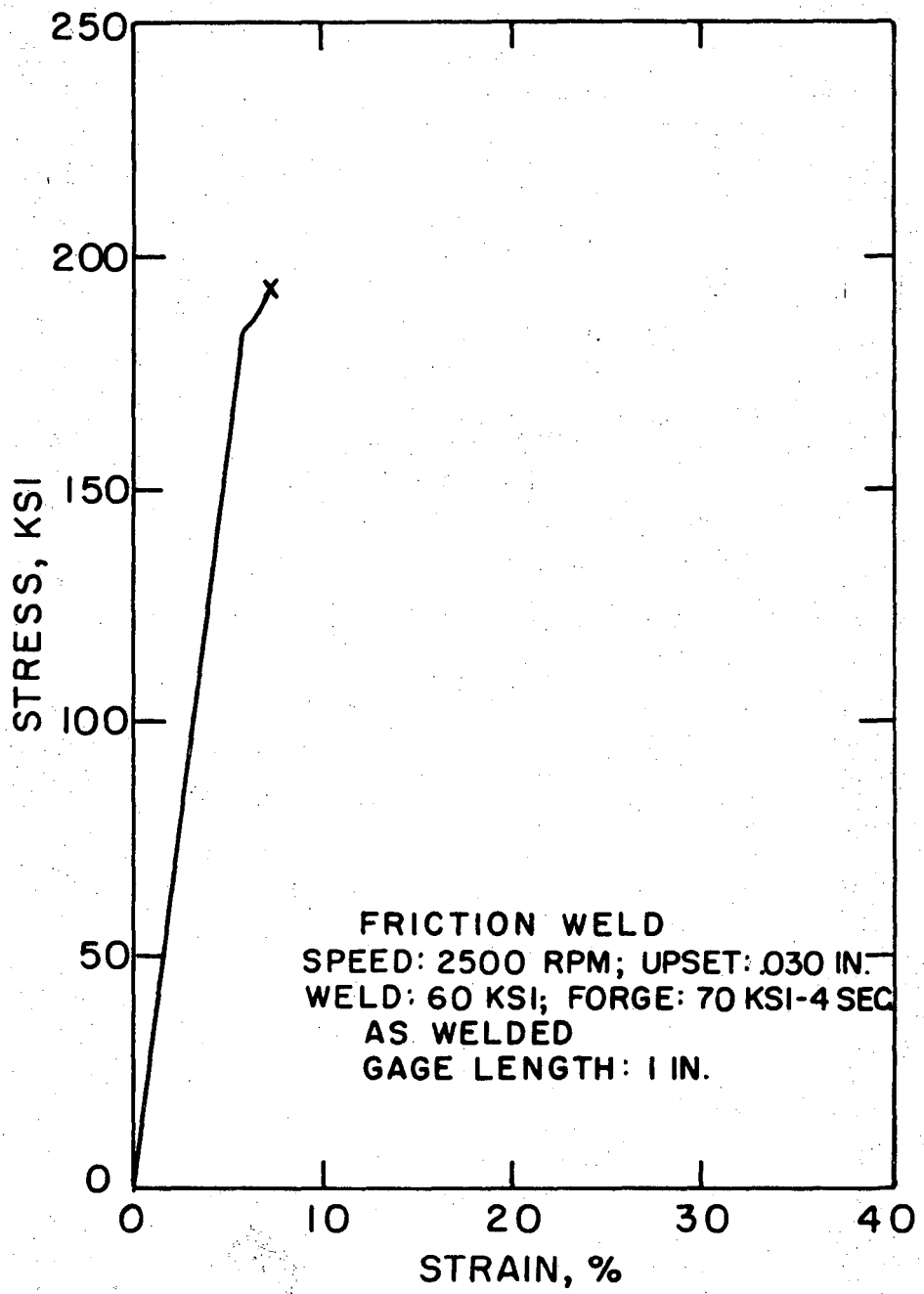

XBL 701-110

Fig. 38

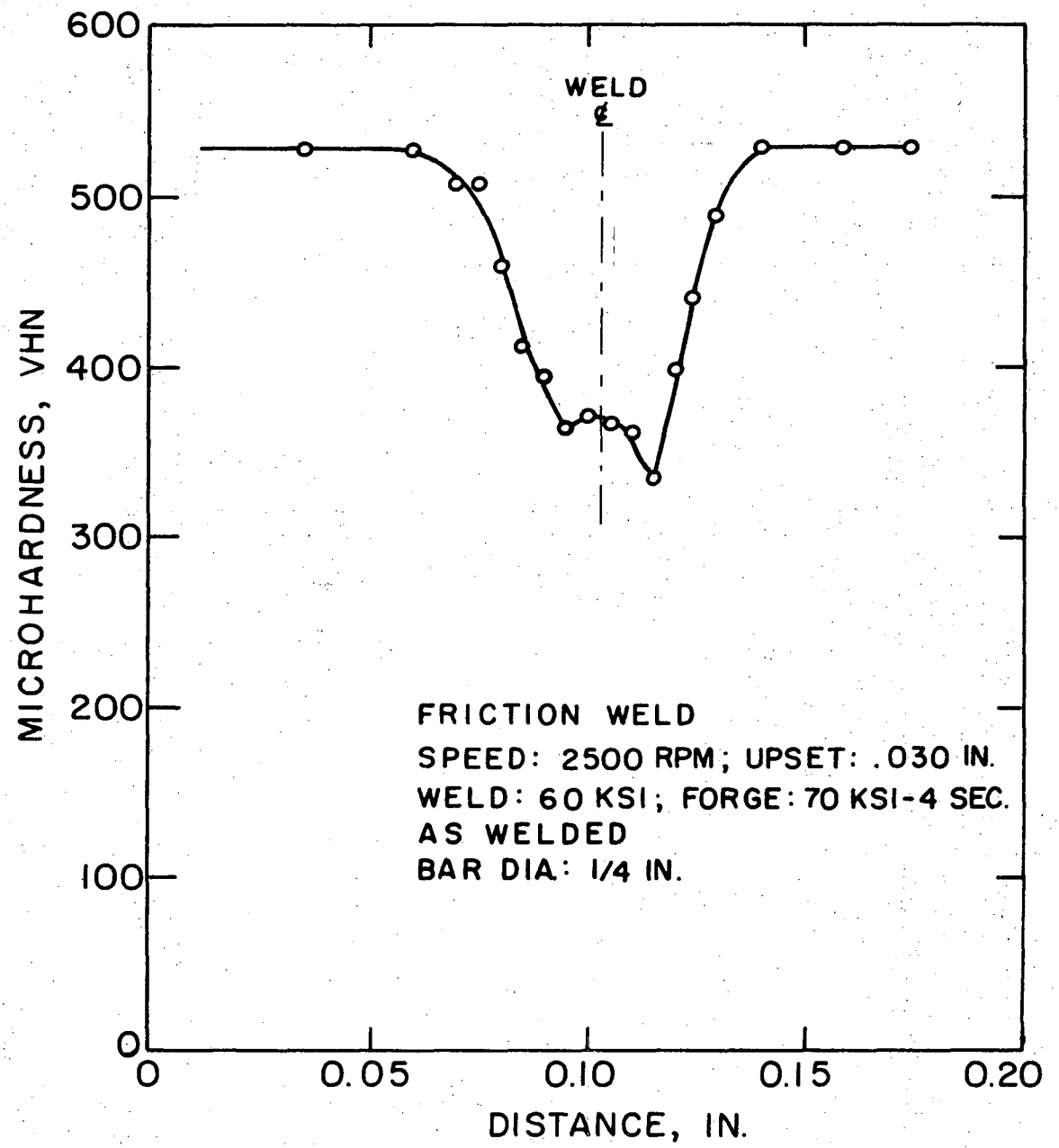

XBL 701-92

Fig. 39

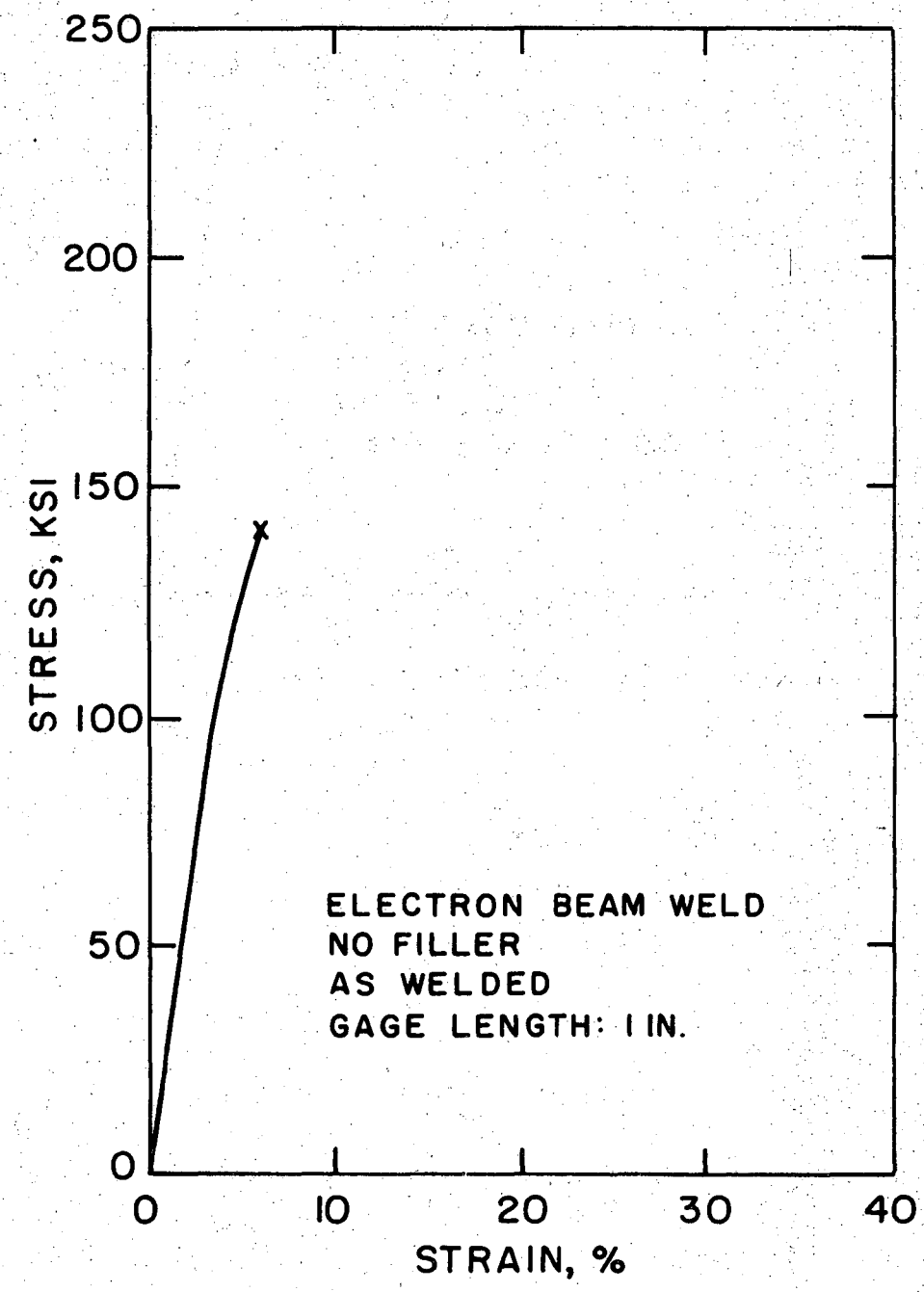

XBL 701-100

Fig. 40

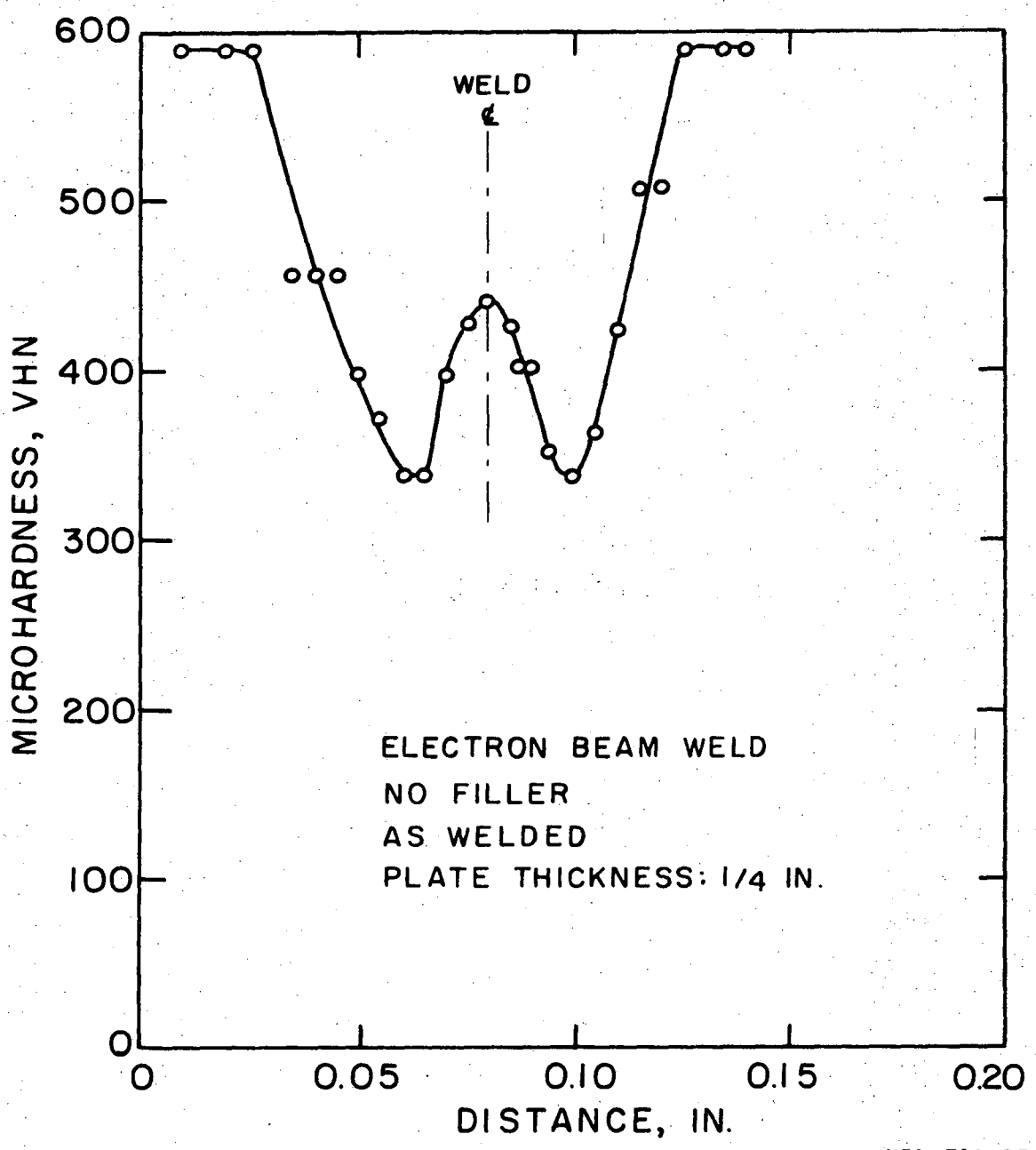

XBL 701-93

Fig. 41

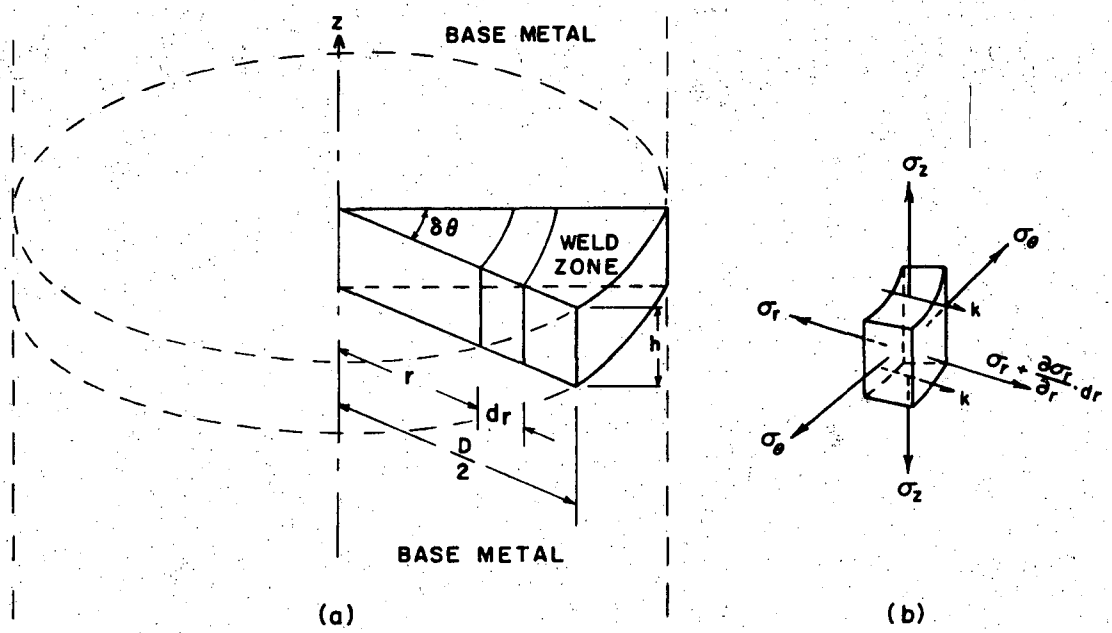

XBL 701-108

Fig. 42

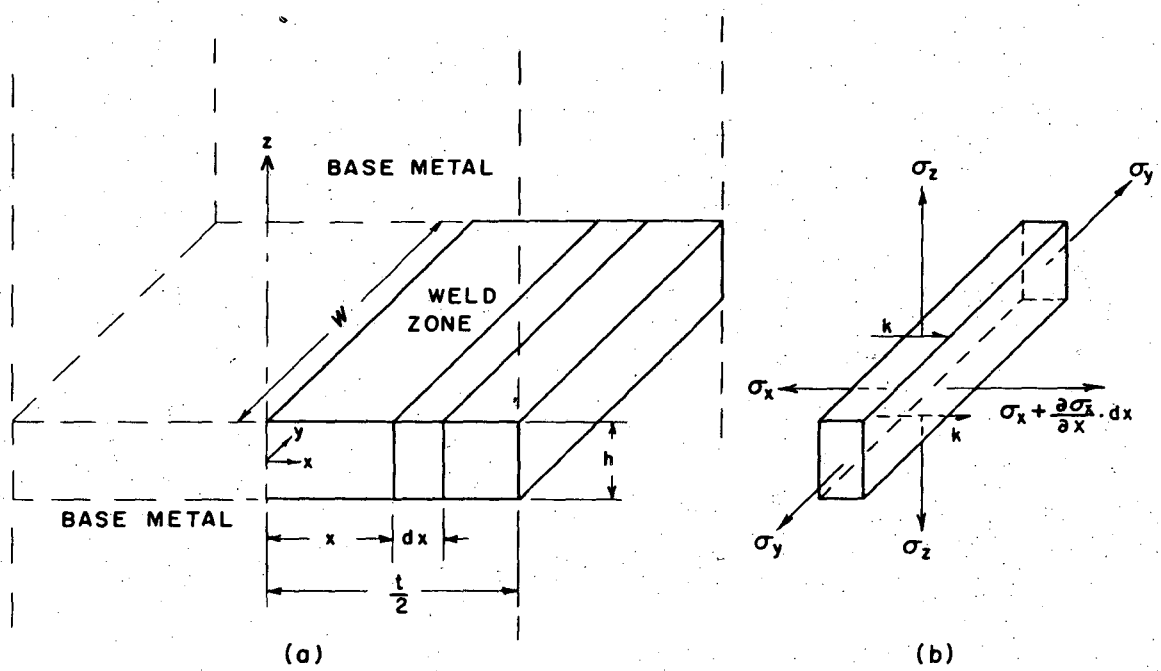

XBL 701-99

Fig. 43

LEGAL NOTICE

This report was prepared as an account of Government sponsored work. Neither the United States, nor the Commission, nor any person acting on behalf of the Commission:

A. Makes any warranty or representation, expressed or implied, with respect to the accuracy, completeness, or usefulness of the information contained in this report, or that the use of any information, apparatus, method, or process disclosed in this report may not infringe privately owned rights; or

B. Assumes any liabilities with respect to the use of, or for damages resulting from the use of any information, apparatus, method, or process disclosed in this report.

As used in the above, "person acting on behalf of the Commission" includes any employee or contractor of the Commission, or employee of such contractor, to the extent that such employee or contractor of the Commission, or employee of such contractor prepares, disseminates, or provides access to, any information pursuant to his employment or contract with the Commission, or his employment with such contractor.

TECHNICAL INFORMATION DIVISION
LAWRENCE RADIATION LABORATORY
UNIVERSITY OF CALIFORNIA
BERKELEY, CALIFORNIA 94720